AN ABSTRACT OF THE THESIS OF

Masahiro Kuno for the degree of Master of Science in Material Science presented on March 15, 2001. Title: Thermodynamics of The $Pd_{43}Ni_{10}Cu_{27}P_{20}$ Metallic Glass-Forming Alloy.

Redacted for Privacy

Abstract approved:_____

Ralf Busch

By the investigation of the bulk metallic glass-forming liquids that have very low critical cooling rates, the thermodynamics of metallic glasses can be clarified. For studying thermodynamic properties, such as the specific heat capacity, calorimetry (DSC) is utilized and one of the most used instruments is the differential scanning calorimeter. In this study calorimetry was used to investigate the thermodynamics of the $Pd_{43}Ni_{10}Cu_{27}P_{20}$ alloy. The specific heat capacity of the liquid and crystalline state, enthalpy, entropy, as well as Gibbs free energy difference between the liquid and crystalline state were measured and evaluated in comparison with previous studies of the alloy. The $Pd_{43}Ni_{10}Cu_{27}P_{20}$ alloy is known as a metallic glass-forming alloy that has high ability for vitrification without crystallization. By observing the onset of heat flux of the exothermic reactions in the DSC, the time-temperature-transformation diagram can be constructed, and the diagram confirms the high ability for the vitrification for the sample. In addition, the effect of fluxing by B_2O_3 to reduce

heterogeneous nucleation is determined by the TTT-diagram. The enthalpy change during the crystallization was directly measured in experiments in which the sample was held isothermally in the DSC. Both enthalpies, calculated from the specific heat capacity measurements and direct measured enthalpy exactly match each other. The very interesting effect in these experiments is an effect of heat treatment in the samples. Two glass transition temperatures can be noticeably recognized by scanning the exothermic event of the sample with the DSC. The material separates into two undercooled liquids. The two phases that are separated during heat treatment can be described by two different fragility parameters.

Thermodynamics of The $Pd_{43}Ni_{10}Cu_{27}P_{20}$ Metallic Glass-Forming Alloy.

by

Masahiro Kuno

A THESIS

submitted to

Oregon State University

In partial fulfillment of
the requirements for the
degree of

Master of Science

Presented March 15, 2001
Commencement June 2001

Master of Science of thesis of Masahiro Kuno presented on March 15, 2001.

APPROVED:

Redacted for Privacy

Major Professor, representing Materials Science

Redacted for Privacy

Coordinator of The Materials Science Program

Redacted for Privacy

Dean of Graduate School

I understand that my thesis will become part of the permanent collection of Oregon State University libraries. My signature below authorizes release of my thesis to any reader upon request.

Redacted for Privacy

Masahiro Kuno, Author

ACKNOWLEGEMENT

Since I began to study in the Mechanical Engineering Department at Oregon State University, many faculty members and friends helped me during my studies. In addition, some friends and a Professor in California Institute of Technology spent time for me to support my research. I deeply appreciate their support and kindness.

First, Dr Ralf Busch has been my advisor since I started my research. He guided me to the goal with accurate advice throughout the years. In addition, he offered the big opportunity to me that I could do research at Caltech. Without him, I could not have deeply understand and completed my research. I also would like to thank Dr. William H. Warnes who also supported and advised me since the beginning of my program.

My appreciation is also for Dr. William L. Johnson because he allowed me to do research and use his facilities at Caltech. Dr. Jan Schroers was especially helpful during my work with the differential scanning calorimeter. Additionally, I want to thank my friends and office-mates, Fred Ellsworth, Ivan McCracken, as well as Isabella Gallino who supported and helped.

Finally, I would like to express my biggest appreciation to my family, especially my parents. Without their encouragement and support with love, I couldn't have achieved my goal and success.

TABLE OF CONTENTS

LIST OF FIGURES

LIST OF FIGURES (Continued)

LIST OF FIGURES (Continued)

LIST OF TABLES

THERMODYNAMICS OF THE $Pd_{43}Ni_{10}Cu_{27}P_{20}$ METALLIC GLASS-FORMING ALLOY.

1.INTRODUCTION

Since the first metallic glass, $Au_{75}Si_{25}$, was investigated by Duwez [1] in 1960 using a rapid quenching method with cooling rate of ~10^6 K/s, thousands of metallic glass have been discovered and studied by many researchers as a new scientific subject. A metallic glass is an amorphous solid, which has no long-range order and is different from a crystalline solid. The glass is vitrified from the liquid by continuous undercooling of the liquid. The properties of metallic glasses have been investigated by many researches and they are very different thermodynamically and mechanically from crystalline solid and they have interesting features. Even though metallic glasses are called glasses, they are not brittle. In addition, the elastic limit is much higher than crystalline solid. Other significant properties are high toughness, hardness, better soft magnetism, high corrosion resistance, low coefficient of friction, high electrical resistance, high viscosity. Most metallic glass-forming alloys cannot be practically used because of processing limitations. There are many methods to make amorphous solids, including sputtering, thermal evaporation, irradiation, or melt quenching. For producing bulk metallic glass, melt quenching is the most popular method. The critical cooling rate determines the thickness of bulk metallic glass. The thickness of metallic glass is proportional to inverse square root of critical cooling rate, *R*.

$$Thickness \propto \frac{1}{\sqrt{R}} \tag{1}$$

As a result, the thickness of achievable sample size does not depend on processing methods, but on the critical cooling rate, which is characteristic for the material. Since Inoue and co-workers [2] discovered metallic glass-forming alloys with a critical cooling rate of 10^2 K/s in the early 1990's, many metastable metallic glass-forming alloys have been discovered, such as Zr-Ti-Cu-Ni-Be alloy introduced by Peker and Johnson [3] at the California Institute of Technology. This Zr-based alloy has a very low critical cooling rate of 1 K/s [4]. The development of more thermally stable new metallic glasses, which form at lower cooling rates, allows for the study of thermal effects from the supercooled liquid state to the crystalline state as well as in the glass transition region. By studying thermodynamic properties, specific heat capacity, viscosity, the atomic diffusion coefficient, and other thermal properties, phenomenon of glass formation and ability of glass forming can be clarified. One way to define glass-forming ability is the ratio between melting temperature and glass transition temperature. The smaller the interval between glass transition temperature and the melting temperature, the greater is the ability for glass formation. The glass transition is the temperature region in which the supercooled liquid freezes to a glass. Using a differential scanning calorimeter (DSC), thermodynamic and kinetic properties as well as thermal events can be determined. The time-temperature-transformation diagram reflects the glass-forming ability. Figure 1 represents 2 different curves: the interval represented in curve (a) has poor glass forming ability because the critical cooling rate of approximately 10^6 K/s is required to avoid crystallization; curve (b) is further from

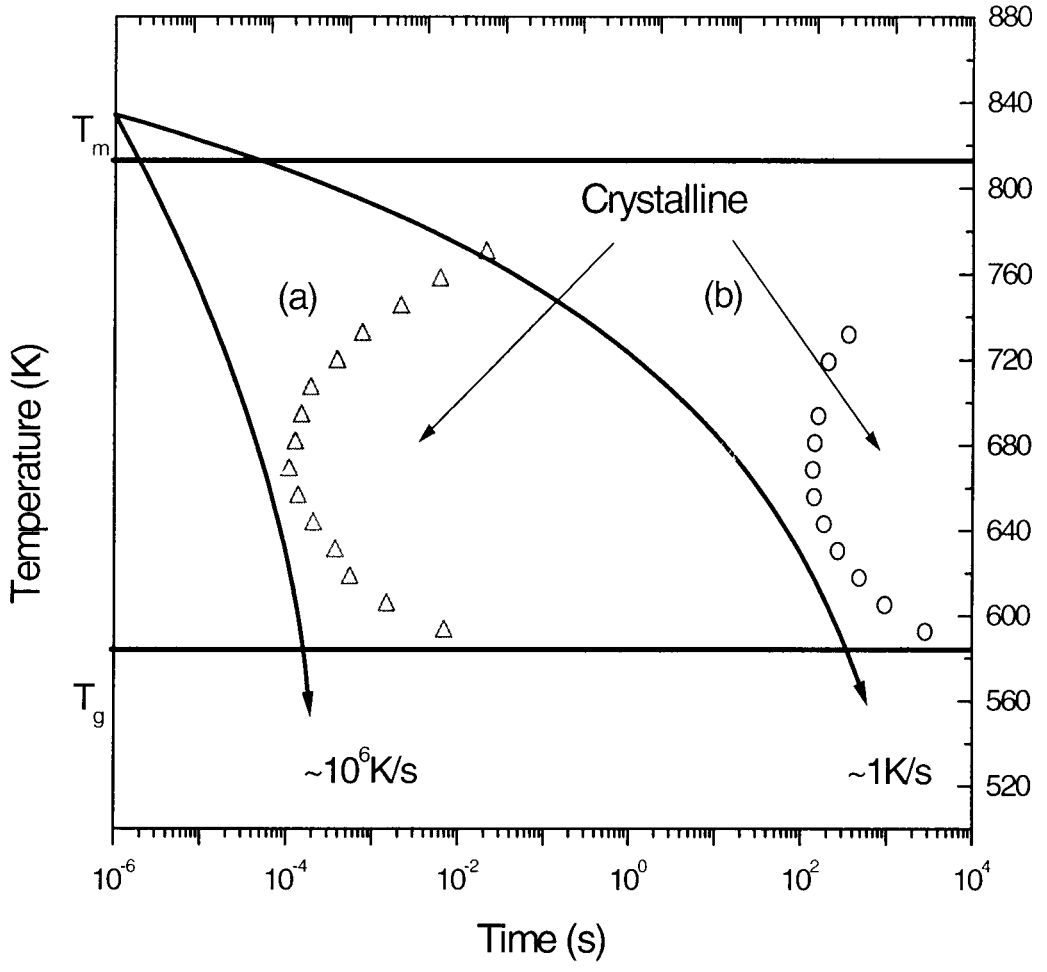

Figure 1: Schematic time-temperature-transformation diagram for (a) a binary metallic glass-forming alloy and (b) a $Pd_{43}Ni_{10}Cu_{27}P_{20}$ non-annealed sample. The two curves with arrows indicate the cooling history needed for glass formation in each alloys.

curve (a) to right, and allows a slow cooling rate, 10^{-1} K/s. A good metallic glass-forming alloy has a TTT diagram like curve (b) in Figure 1. The better metallic glass-forming alloys have slower critical cooling rates, and the compositions of those alloys are strongly related to deep eutectics [5]. Inoue suggested three rules for glass formation in metallic systems [6]. First, the alloys have to consist of at least three elements. Second, the atomic sizes of the elements should have at least 12 % difference between the largest and smallest atom. Third, the elements have to have a large negative heat of mixing. A.L. Greer explains the first two rules [7]. In the $Pd_{43}Ni_{10}Cu_{27}P_{20}$ alloys, for example, the radius of Pd is 0.138 nm, of Ni 0.125 nm, of Cu 0.128 nm, and of P 0.111 nm. The difference in atomic size is over 12 % between copper and phosphorus, and the material is a multicomponent alloy. The crystallization in the multicomponent alloys is suppressed indicating that increasing complexity improves the glass-forming ability. The liquid phase is stabilized with respect to the crystalline solid reducing the melting temperature in the system with deep eutectics. The lower melting temperature reduces the interval between the glass transition temperature and the melting temperature. The nucleation and growth of crystals is suppressed with a smaller temperature interval to form crystals. The alloy, which has a composition near a deep eutectic, has better metallic glass-forming ability.

The $Pd_{43}Ni_{10}Cu_{27}P_{20}$, alloy has been discovered by Lu and co-workers [8]. Some thermodynamic properties and heats of transformation were reported, indicating a good ability for glass formation. In the present study, the thermodynamic properties are further investigated. The $Pd_{43}Ni_{10}Cu_{27}P_{20}$ alloy has been heat treated from 473 K

to 633 K with a heating rate of 0.333 K/s. The thermodynamic functions of these alloys as a function of temperature are measured. This results on the specific heat capacity, enthalpy, entropy, and Gibbs free energy difference between liquid and crystalline state are presented. The time scale for the crystallization under isothermal condition can be provided by the time-temperature-transformation diagram (TTT diagram). The TTT diagram gives us information about the time that a cooled metallic glass-forming alloy needs to reach a certain amount of crystallization in an experiment as a function of temperature. The most typical characteristic of the TTT-diagram is the crystallization nose that represents the crossover of decreasing nucleation barrier and the slowdown of the kinetics of the undercooled melt So far, only some TTT diagrams for metallic glass-forming alloys have been reported, such as for $Zr_{41.2}Ti_{14}Cu_{12}Ni_{10}Be_{23}$ [9]. The ability for glass formation is defined as the ability not to crystallize when an alloy is cooled from the equilibrium liquid state to glass transition temperature. A good metallic glass-forming alloy must have the lower critical cooling rates compared to metallic glass-forming alloys, which have a poor ability of glass transformation. In this study the enthalpy change from the liquid to the solid of an undercooled liquid is determined experimentally for the first time in the entire temperature interval from the melting point to the glass transition. In this thesis, the thermodynamic properties, ability of glass formation, and effect of heat treatment on the $Pd_{43}Ni_{10}Cu_{27}P_{20}$ alloy are discussed.

2. EXPERIMENTAL METHOD

2.1 Sample Preparation

There are several methods to produce amorphous solids, such as sputtering, thermal evaporation, or melt quenching. In this study, amorphous samples were prepared by inductively melting the constituents (purity ranging from 99 % to 99.999 %) in quartz tubes for 20 min at 1200 K followed by water quenching. The samples were fluxed in B_2O_3, which was previously dehydrated for 3 hours at 1200 K. Wavelength-dispersive-spectrometer X-ray measurements were carried out to verify the composition of the samples. Glassy samples, $Pd_{43}Ni_{10}Cu_{27}P_{20}$, up to 70 mg and an additional few mg of B_2O_3 for the flux experiments were introduced into graphite crucibles and processed in a DSC (Perkin Elmer).

2.2 Differential Scanning Calorimeter

In the Differential Scanning Calorimeter (DSC), a sample and an inert reference material are subjected to an identical thermal treatment. In the case of a reaction or transformation in the sample, a heat flux is generated that corresponds to the energy associated with the type of transition, which can be exothermic or endothermic. Using a DSC, thermal effects can be measured as peaks or thermal transitions on different time scales by changing the heating rate or cooling rate. The

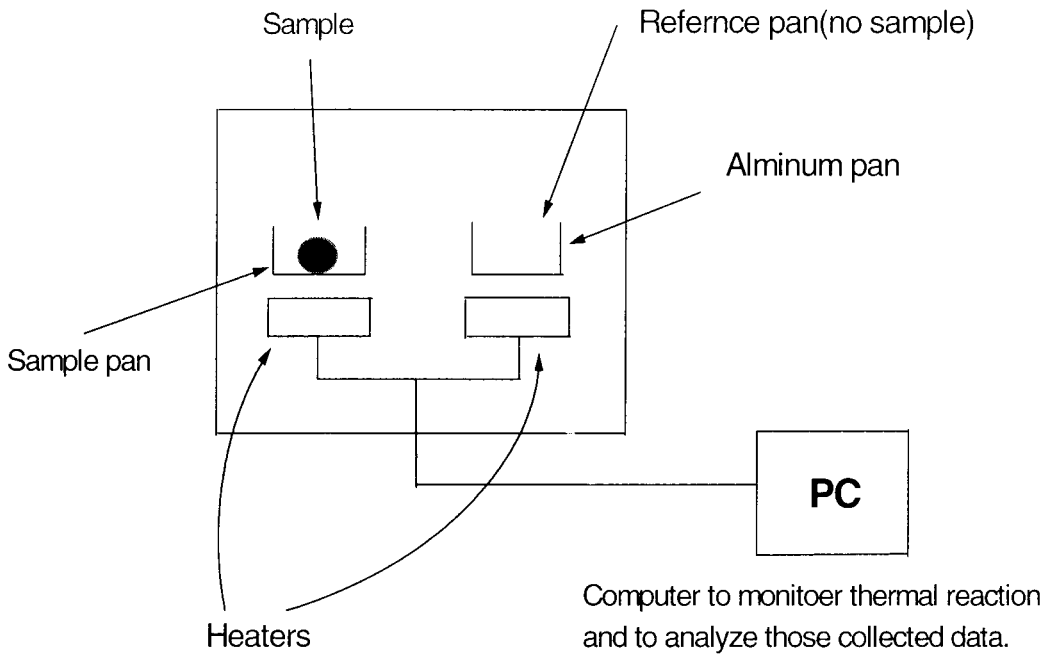

Figure 2: Schematic diagram of the DSC.

kinetic parameters can, therefore, be characterized both qualitatively and quantitatively. In this work, a Perkin Elmer DSC7 is used to determine the thermodynamics and kinetics of $Pd_{43}Ni_{10}Cu_{27}P_{20}$ alloys.

This DSC7 has two furnaces that are thermally isolated. Two containers (pans) are needed to do the measurement accurately. One is for the sample and another is for the reference that must be empty [10]. Figure 2 indicates a schematic diagram of the

DSC. The sample and reference are thermally insulated with respect to each other. Each furnace is heated by an individual heater at the same rate. Both furnaces are always kept at the same temperature.

To avoid oxidation during the measurements, both pans are kept in argon atmosphere. The aluminum pans were used to hold the samples, if measurements were done below the melting point of the $Pd_{43}Ni_{10}Cu_{27}P_{20}$ alloy. Graphite crucibles alternative pans instead of the aluminum pans were used, when the sample needed to be heated above the melting temperature of $Pd_{43}Ni_{10}Cu_{27}P_{20}$. When the graphite crucibles were used in the DSC, the sample size was confined in a height to 2 mm and a weight of less than 65 mg.

2.3 Calibration

Calibration has to be done to check the precision and accuracy of the equipment. The baseline of the DSC must be calibrated to ensure that it is performing as it is designed. This operation is usually performed initially by the equipment manufacturers. To insure the integrity of the data, periodic recalibrations of the baseline have to be performed. The baseline was corrected prior to the experiments that are presented in this study. In addition, the temperature and heat flow have to be calibrated. The standard method of temperature calibration is that the melting temperature of certain high purity metals is measured. The peak temperature and peak

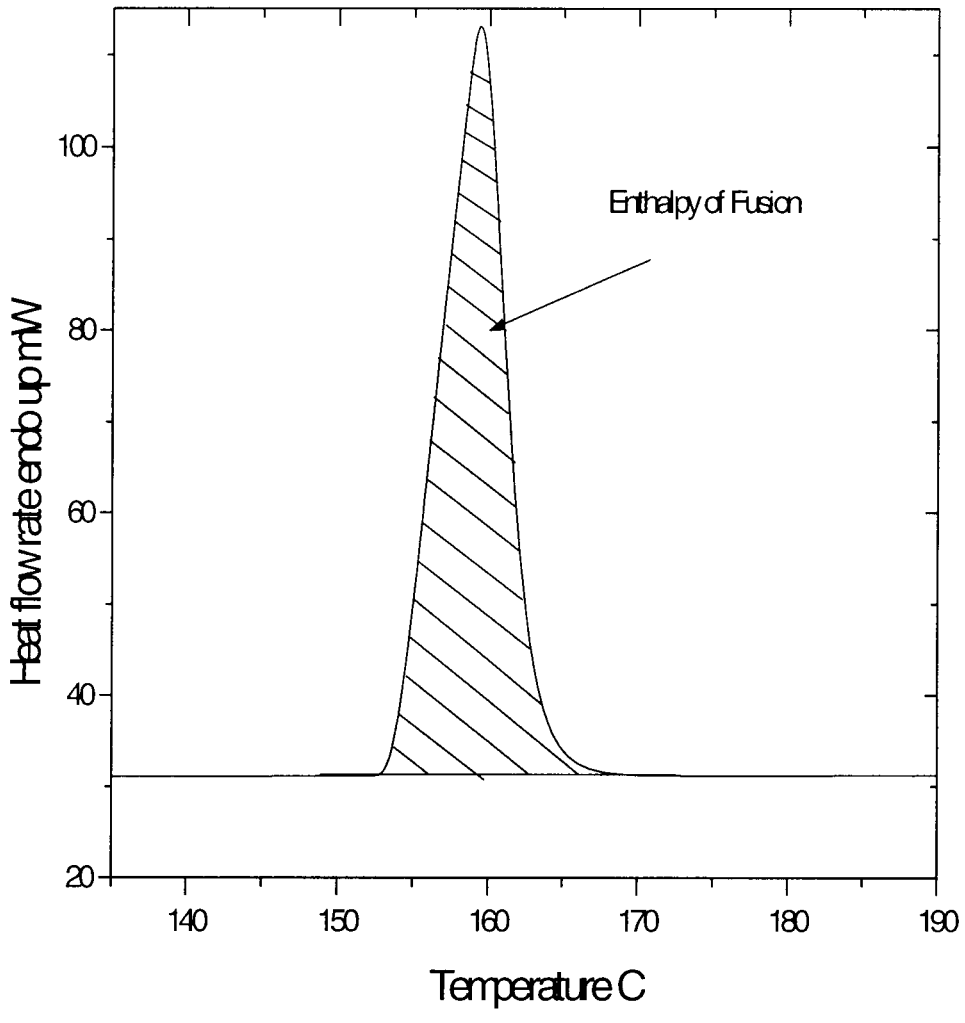

Figure 3: DSC scan for an enthalpy measurement of indium. The peak area indicates the enthalpy of fusion.

areas are then determined and serve as calibration parameters for the software. In this study, indium and zinc were used as calibration standards. The calibration of the temperature is essentially based on the determination of the extrapolated peak onset temperature, measured at different heating and cooling rates. The temperature calibration was performed for different heating rates, from 1 K/min to 280 K/min, using indium and zinc standards with a high purity of 99 % to 99.999 %. For indium, in addition, the enthalpy of the fusion, which is the peak area, was determined. The zinc was heated from 325 K to 823 K to determine the melting temperature, which is 693K. The onset of the melting peak is determined as the melting temperature for zinc as a function of heating rate. For indium, the same procedure as for zinc was carried out. A typical melting peak for indium is indicated in Figure 3. The difference of enthalpy of fusion is determined by calculating the area of heat of fusion. The enthalpy of fusion of indium shifts linearly with changing heating rate as can be seen in Figure 4. The result of the calibration data for zinc and indium were plotted and extrapolated to determine the relation of heating rate and melting temperature shift. Figure 5 and 6 show the linear fit for the shift in temperature for indium and zinc, respectively.

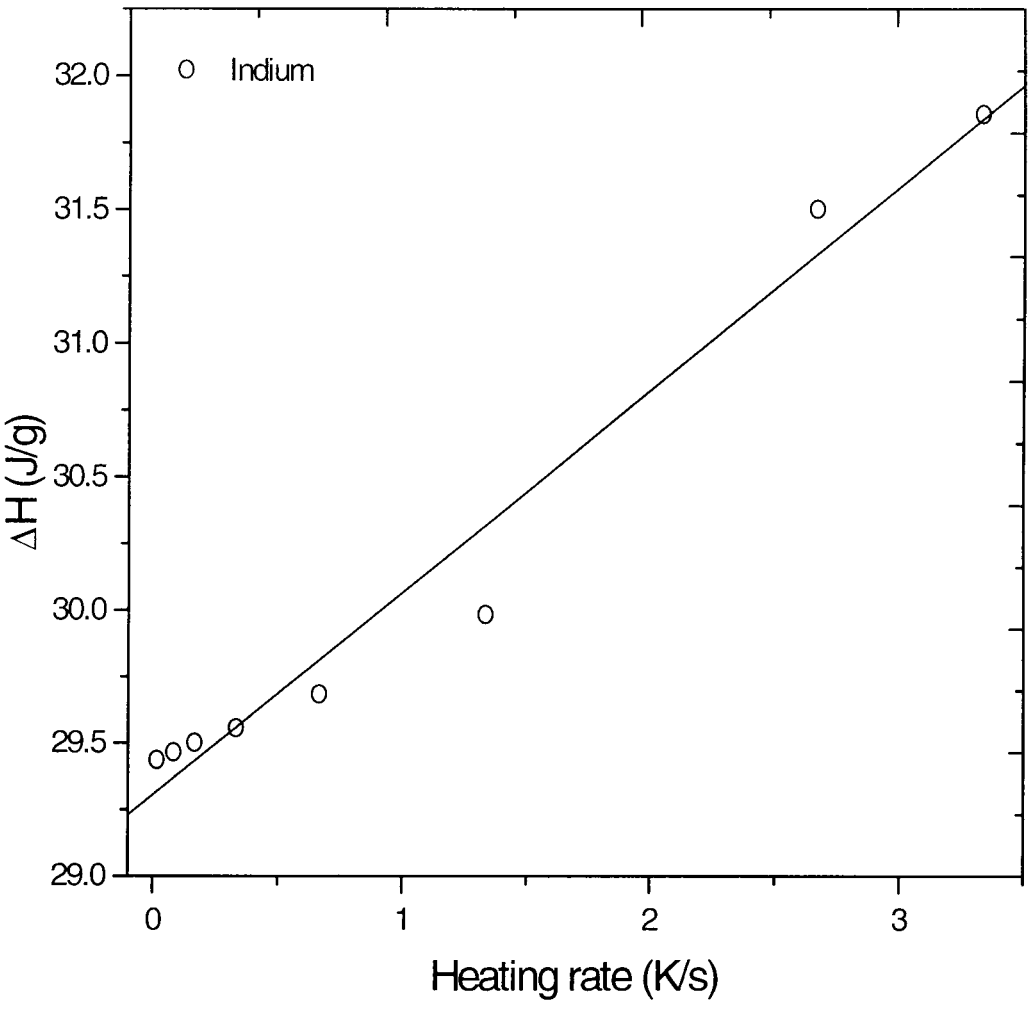

Figure 4: The calibration data for the enthalpy of an indium standard.

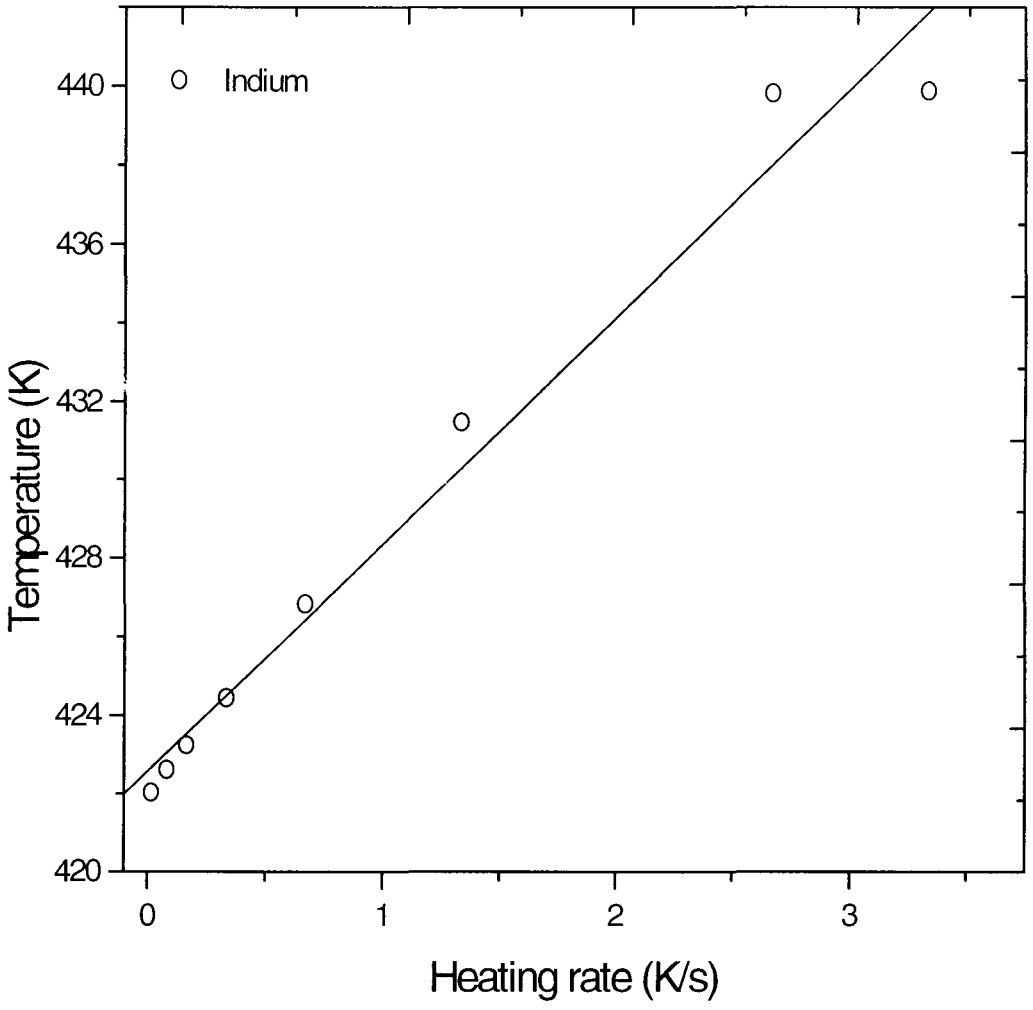

Figure 5: The temperature calibration data for an indium standard.

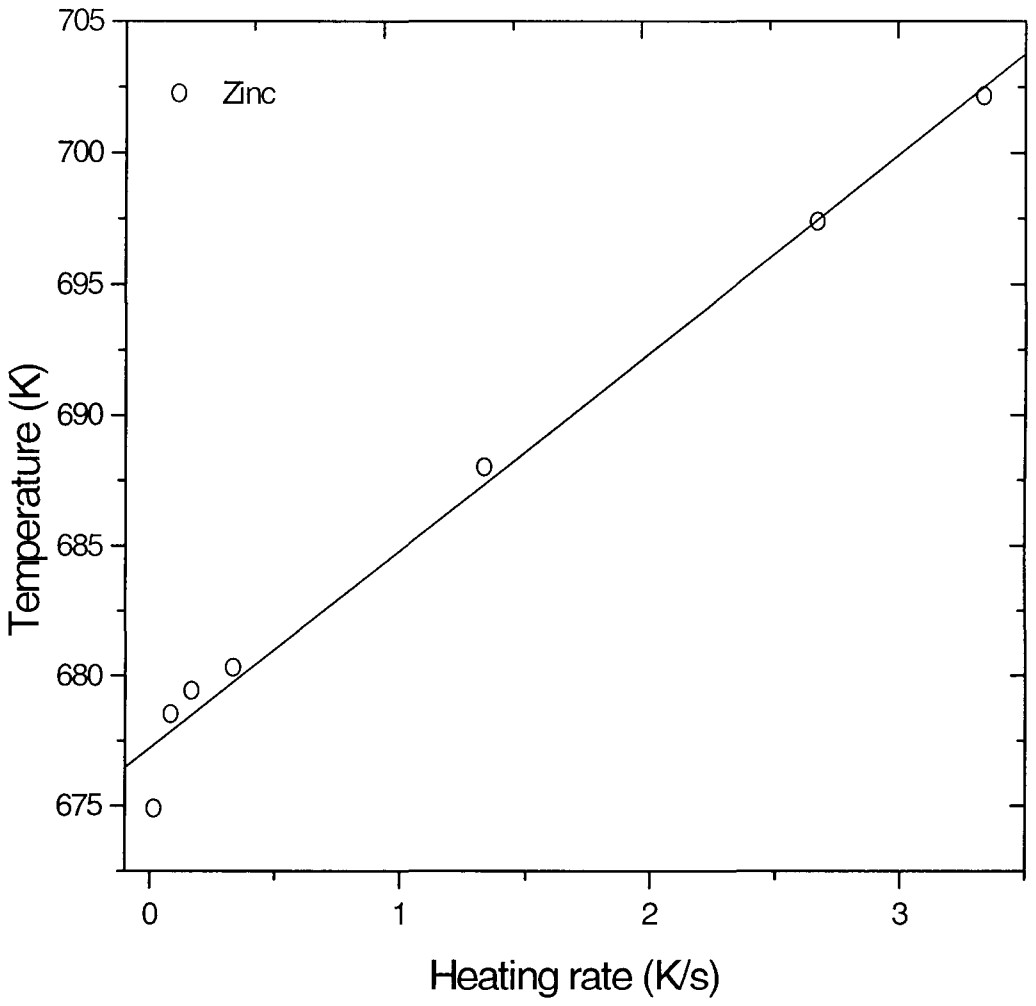

Figure 6: The temperature calibration data for the zinc standard.

2.4 Specific Heat Capacity

The specific heat capacity is defined as the amount of heat that is required to raise the temperature of one mole of a substance one Kelvin. Because the heat capacities of most materials vary with changing the temperature, the temperatures of both the specified substance and the reference substance must be known in order to give a precise value for the specific heat. In this work we measured the heat flow for the $Pd_{43}Ni_{10}Cu_{27}P_{20}$ alloy, empty pan, and sapphire as standard material, and determined the specific heat capacity of the $Pd_{43}Ni_{10}Cu_{27}P_{20}$ alloy in reference to this standard.

The $Pd_{43}Ni_{10}Cu_{27}P_{20}$ alloys were produced by Schoers and Busch [10] as described in chapter 2-1. The calibration of zinc and indium was done for a heating rate of 0.333 K/s in this study. The specific heat capacity of the crystallized sample was determined between 350 K and 770 K below the melting point, and the specific heat capacity of the liquid was measured up to 950 K. The measurements, for sapphire and the empty pan, followed the same temperature range as the measurement for the $Pd_{43}Ni_{10}Cu_{27}P_{20}$ alloys. The heat flow at a certain temperature for both the crystalline and liquid state was measured by heating with a fixed rate from a temperature T_1 to a temperature T_2, and stopping at T_2. The schematic specific heat capacity measurement with DSC is shown in Figure. 7 [11][12]. The $\frac{dQ}{dt}$ is the difference in heat flow after heating from a temperature T_1 to a temperature T_2, and holding at T_2. The heat flow is shown in unit of heat, Q per unit time, t. In this work

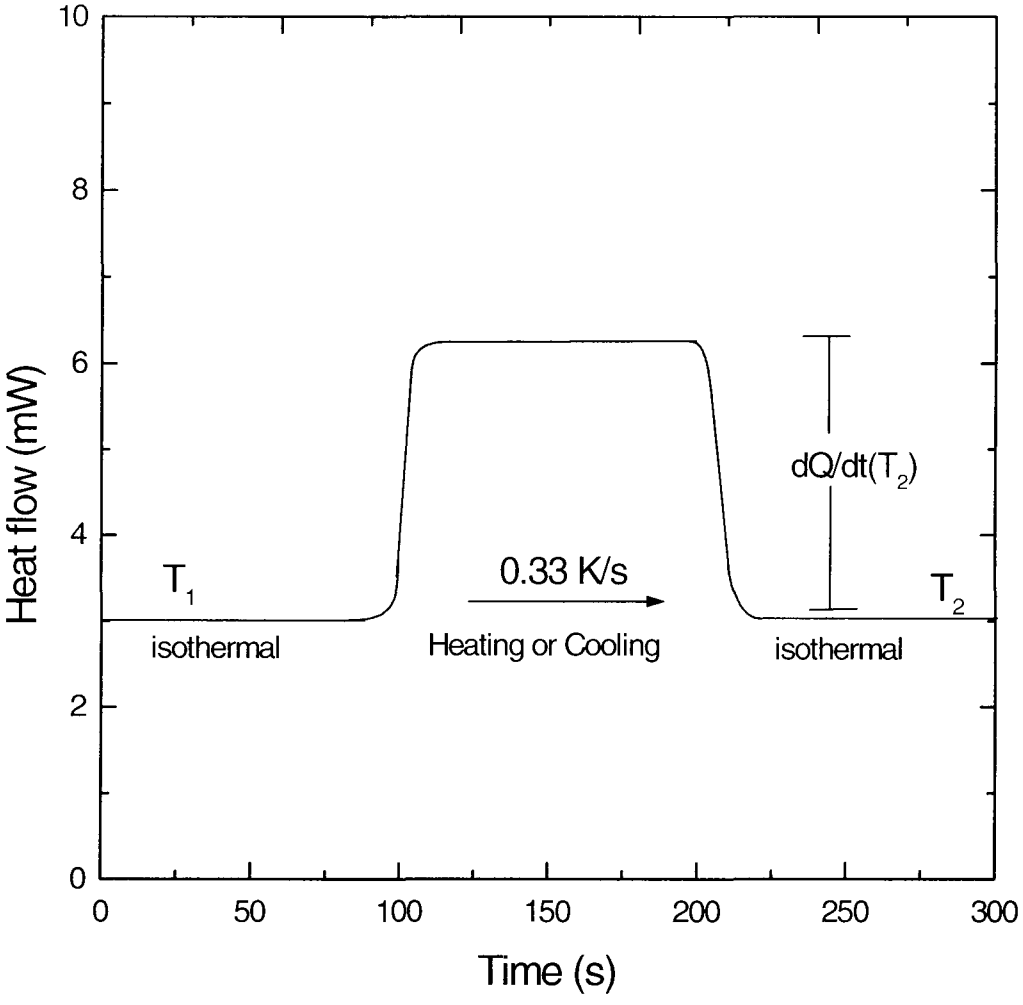

Figure 7: Typical specific heat capacity measurement with the DSC at the certain temperature.

we used J/g-atom-K as unit. The unit g-atom replaces mole in alloys, because we do not have compounds of fixed geometry. The heating rate is temperature increase, T, per unit time, t. The heat capacity temperature. was measured during heating and cooling. By determining the heat supplied by the result of a temperature increase or decrease, the heat capacity can be determined. The heat capacity is determined by the ratio of the quantity of the heat gain or release from system as a result of temperature change.

$$\frac{q}{\Delta T} = C \tag{2}$$

In this study, the heat capacity was measured under the constant pressure. The heating process is that the sample was heated up with a constant rate of 0.33 K/s and then kept steady for 120 seconds. The difference of heat flux $\frac{dQ}{dt}$ is given by

$$\frac{dQ}{dt} = \left(\frac{\partial Q}{\partial t}\right)_{T\neq 0} - \left(\frac{\partial Q}{\partial t}\right)_{T=0} = C \cdot \frac{dT}{dt} \tag{3}$$

where $\left(\frac{\partial Q}{\partial t}\right)_{T\neq 0}$ is the power to heat the sample and the sample pan at each heating rate, $\left(\frac{\partial Q}{\partial t}\right)_{T=0}$ is the power to keep the sample and sample pan at a certain temperature, C is the heat capacity of empty pan and sample. To determine the heat capacity of the sample, sapphire and empty pan itself have to be measured their exothermic heat flow. In addition, the specific heat capacity of sapphire is required to be known as a standard. Finally, the specific heat capacity of sample is calculated by the following equation:

$$c_p(T)_{sample} = \frac{\dot{Q}_{sample} - \dot{Q}_{pan}}{\dot{Q}_{sapphire} - \dot{Q}_{pan}} \cdot \frac{m_{sapphire} \cdot \mu_{sample}}{m_{sample} \cdot \mu_{sapphire}} \cdot c_p(T)_{sapphire} \quad (4)$$

where m is the mass of sapphire and sample, μ is the molar mass of them, and $c_p(T)_{sapphire}$ is the specific heat capacity of sapphire.

2.5 Measurement of The Heat of Fusion on Heating

In a phase change, from a solid state to a liquid state, the change in the enthalpy of the system is the latent heat of fusion. When a solid substance is converted into a liquid, a certain amount of heat is required. This amount of heat is an extensive property and its value is characteristic of the substance. Figure 8 shows DSC scan of typical heat flux vs. temperature diagram around the melting point of the $Pd_{43}Ni_{10}Cu_{27}P_{20}$ alloy. The eutectic temperature, T_{eut} is the temperature at which the solid starts to melt. T_{peak} is the temperature of the melting peak. T_{liquid} is the temperature at which the alloy is completely melted. By integrating the peak area, the enthalpy of fusion can be determined. Using measured data of specific heat capacity in both the liquid and crystalline state, the enthalpy, entropy, and Gibbs free energy were calculated. In addition, those thermodynamic functions give us information for glass forming ability of the $Pd_{43}Ni_{10}Cu_{27}P_{20}$ alloy. The driving force for the crystallization can be determined. One way to determine the glass forming ability is the time-temperature-transformation diagram (TTT diagram). Although the TTT diagram will be explained in more detail in the next chapter, an undercooled

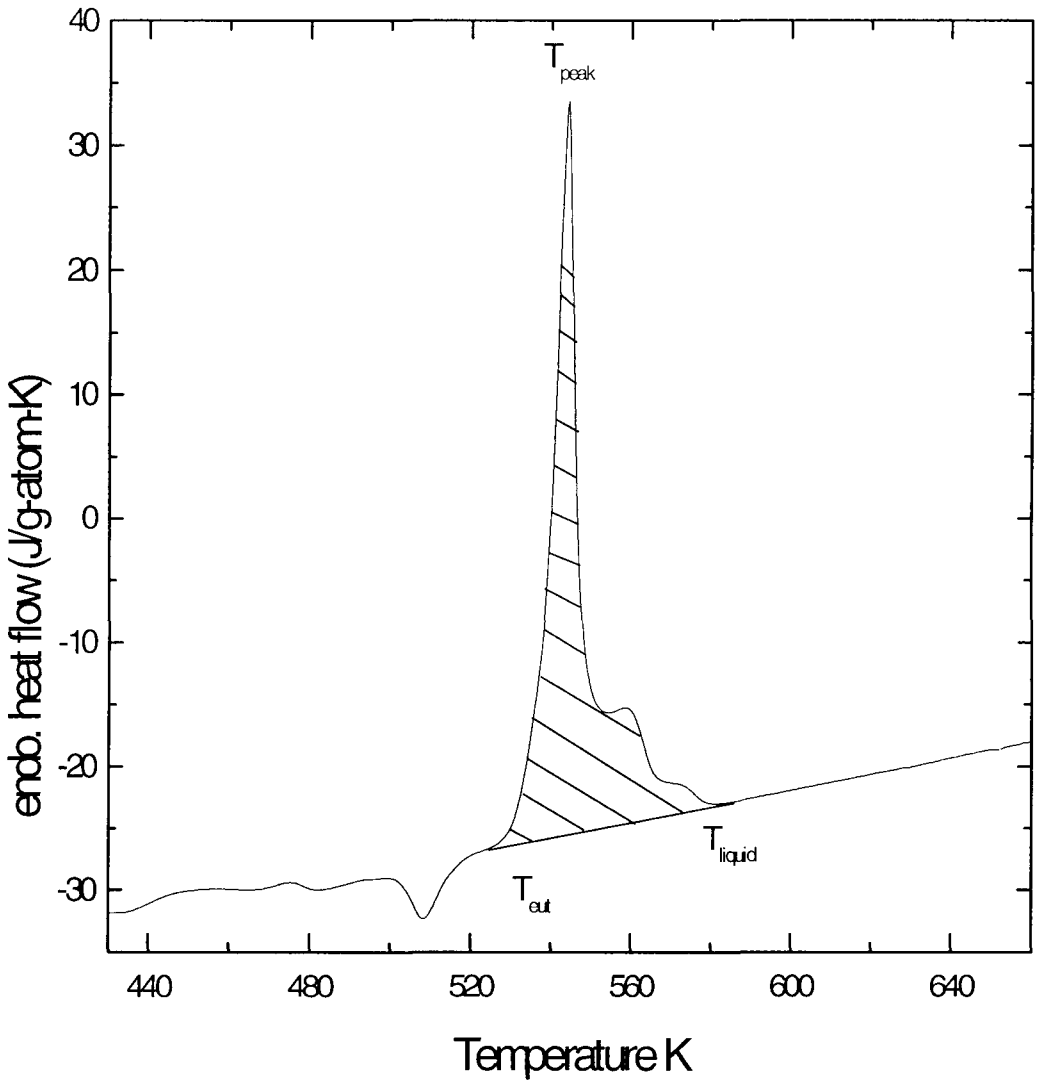

Figure 8: DSC scan of a typical amorphous solid from crystalline state to the liquid state. The dashed area is the heat of fusion, ΔH_f.

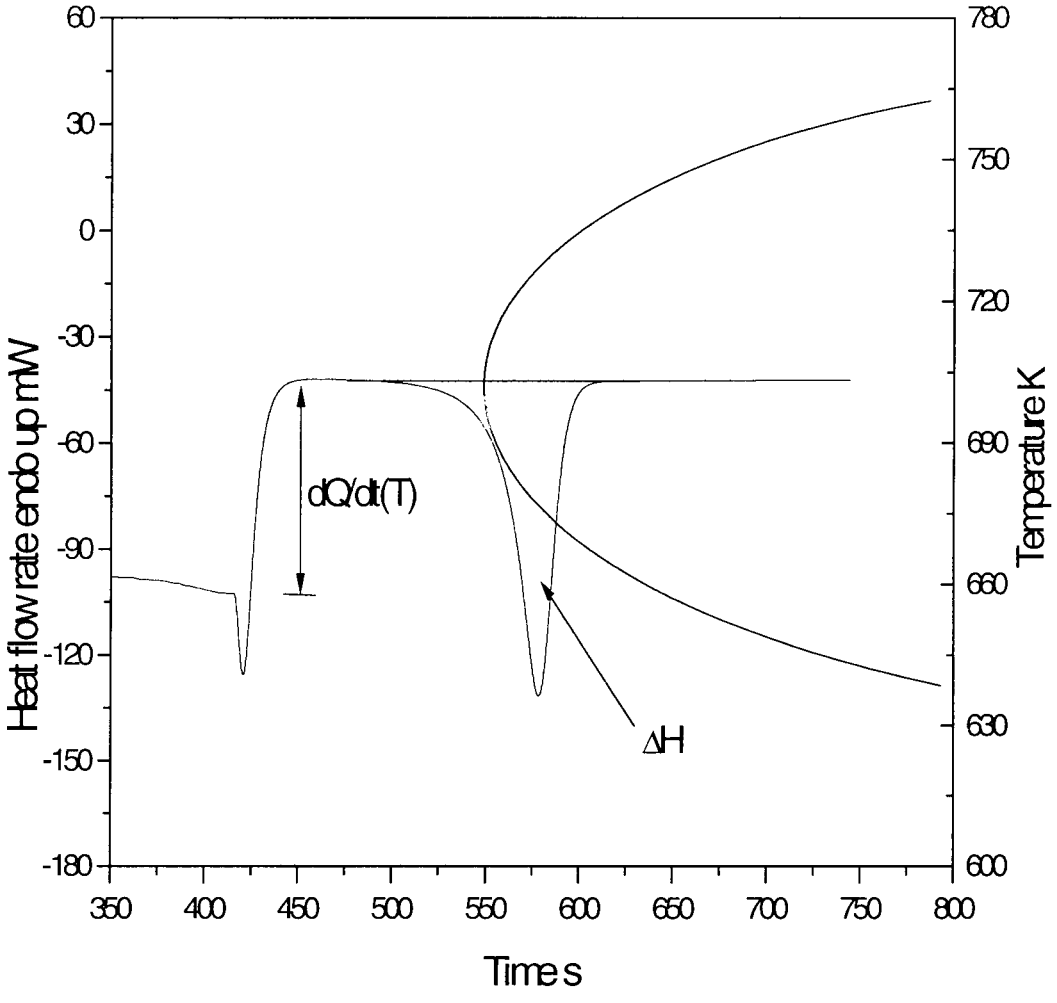

Figure 9: Combined specific heat capacity measurement and isothermal crystallization experiment. The enthalpy of crystallization is measured at 683 K. The time-temperature-transformation curve is drawn in schematically.

experiment for depicting the TTT diagram is shown in Figure 9. In that diagram, the heated sample was cooled down to 693 K then its temperature was kept constant long enough to measure the enthalpy. The nose of time-temperature-transformation curve for 1 % crystallized volume fraction crosses the 1 % of the enthalpy scanning curve.

2.6 Time-Temperature-Transformation Diagram

The time-temperature-transformation diagram (TTT diagram) presents a characterization of the time scale for crystallization under isothermal condition. The TTT diagram presents the thermal stability of undercooled liquid with respect to the crystallization. The onset time for starting crystallization is plotted as a function of temperature in the undercooled liquid in the diagram. The experimental method for plotting the TTT diagram was already shown in Figure 9. The samples were undercooled to a certain temperature with holding isothermally until crystallization started. As it was shown in Figure 1, the TTT diagram is one way to determine glass-forming ability of alloys. The good metallic glass-forming alloys have high resistance against the crystallization of undercooled liquid, and it is proved by TTT diagram. In this study, the $Pd_{43}Ni_{10}Cu_{27}P_{20}$ alloy was measured either with fluxing in B_2O_3 or without any fluxing. As it was shown in the last chapter, the enthalpy change at each temperature determines the TTT diagram. The effect of B_2O_3 fluxing for glass forming ability was studied with Pd-Ni-P alloy with B_2O_3 [13][14]. The crystallized volume fraction as a function of time was studied in the supercooled liquid regime in

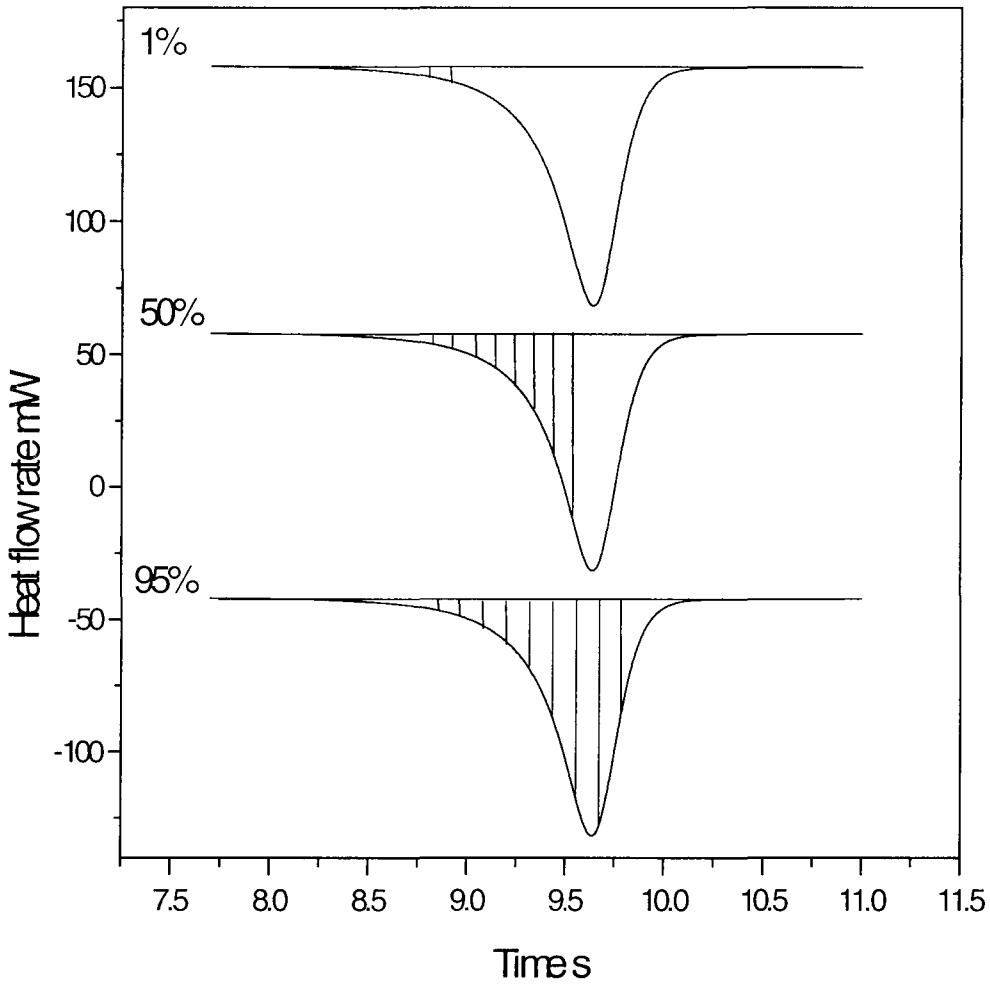

Figure 10: Crystallized volume fraction for 1%, 50%, and 95% function of time.

this experiment. To characterize the crystallization event, 1%, 50%, and 95% of crystalline volume fraction were measured and are shown as a TTT diagram. The crystallized volume fraction is assumed to be proportional to the enthalpy difference that is released. Figure 10 shows those points.

3. RESULT

3.1 Specific Heat Capacity

The specific heat capacity of the glassy $Pd_{43}Ni_{10}Cu_{27}P_{20}$ alloy, the crystalline solid and the supercooled liquid, is shown in Figure 11. The T_g indicates the onset point of the glass transition temperature. T_k indicates the Kauzmann temperature (See chapter 3-2) and T_m indicates the melting temperature of $Pd_{43}Ni_{10}Cu_{27}P_{20}$. The specific heat capacity for the crystalline and the amorphous state was determined by DSC experiments as explained in chapter 2-5. The crystalline state of this alloy consists of multiple phases. The specific heat capacity of the crystalline state almost linearlly increases from 350 K to the eutectic temperature with increasing temperature. To satisfy Kubaschewski's equation, [15] which represents the temperature dependence of the specific heat capacity of the crystalline state far above the Debye temperature, line fit is required and it can be defined by

$$c_p^x(T) = 3R - a \cdot T + bT^2 \tag{6}$$

The specific heat capacity of the liquid is defined by

$$c_p^l(T) = 3R + c \cdot T + d \cdot T^{-2} \tag{7}$$

Where a, b, c, and d are fitting constants, a = 0.0053, b = 0.000019, c = 0.012, d = 4932000, R = 8.31452 J g-atom^{-1} K^{-1}. The solid line in figure, which is $c_p^x(T)$, is an extrapolation fit from the data of the specific heat capacity of the solid. Up to 450 K,

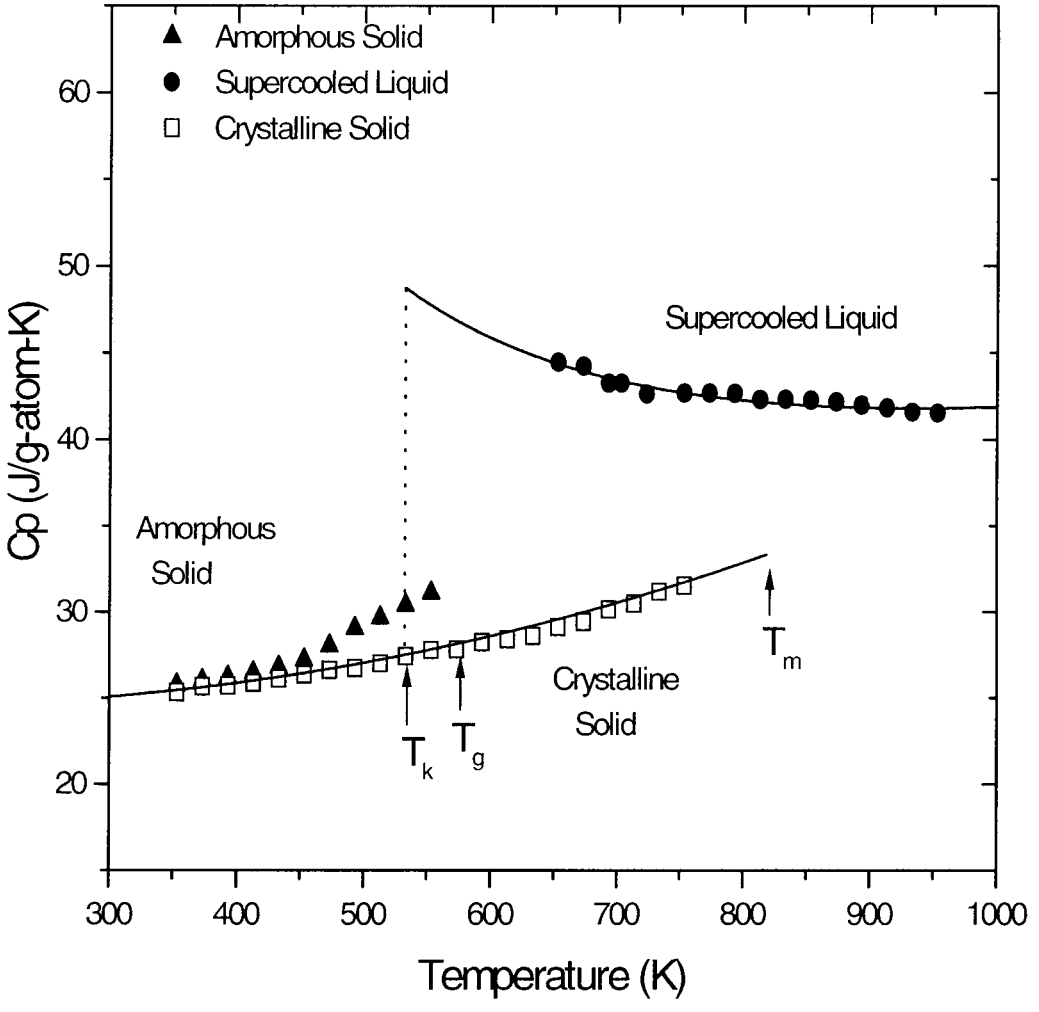

Figure 11: The specific heat capacity of $Pd_{43}Ni_{10}Cu_{27}P_{20}$. The line on the graphs is fitted to Equation (2), and (3). T_k is the Kauzmann temperature, T_g is the glass transition temperature, and T_m is the melting temperature.

the specific heat capacity of the glass is identical to the specific heat capacity of crystalline with increasing temperature. When the temperature gets closer to the glass transition temperature, the specific heat capacity of the glass deviates from that of the crystal. At the glass transition temperature, the specific heat capacity of the glass sharply increases into the supercooled liquid. It reaches the maximum value at around 600 K. At that temperature, the specific heat capacity of supercooled liquid is twice as high as the crystal comparing to the specific heat capacity of it at 350 K. After the specific heat capacity reaches to the maximum value, it decreases slowly with increasing temperature and comes closer to the specific heat capacity of the crystal. It continues to drop in the equilibrium liquid regime. Lu and his co-workers [8] reported lower result of the specific heat capacity of the liquid and the crystal of $Pd_{43}Ni_{10}Cu_{27}P_{20}$ compared to our result.

3.2 Enthalpy, Entropy, and Gibbs Free Energy

The heat of fusion is determined by the peak area of the melting transition. The difference between heat of fusion and heat of crystallization reflects a finite specific heat capacity difference between supercooled liquid and crystalline solid. Figure 11 is a typical specific heat capacity plot of the metallic glass-forming alloy. Using the collected data of $c_p^s(T)$ and $c_p^l(T)$, the change in the thermodynamic functions between the liquid and the crystalline state as a function of temperature is determined. The enthalpy difference is, now, given by

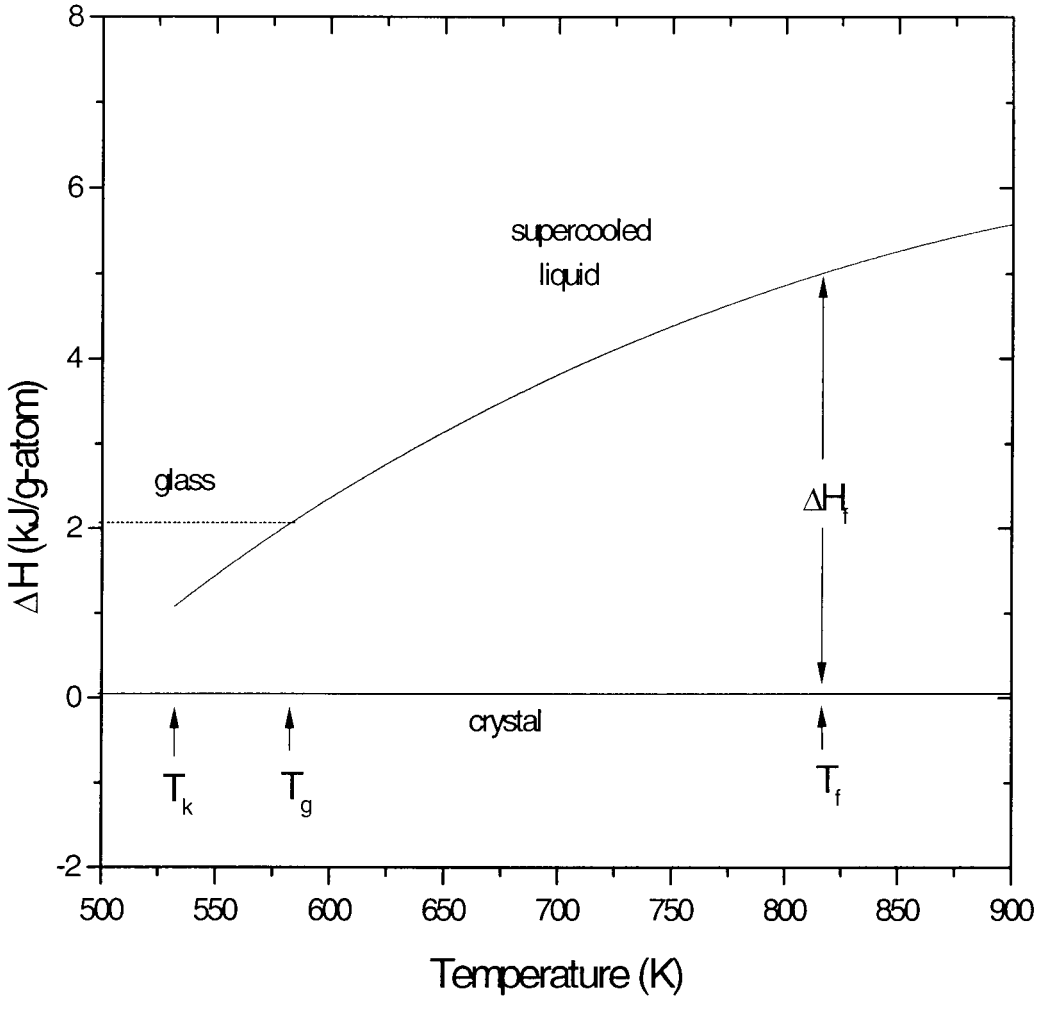

Figure 12: Enthalpy difference between the liquid and crystalline state of $Pd_{43}Ni_{10}Cu_{27}P_{20}$. T_k is the Kauzmann temperature. T_g is the glass transition temperature. T_f is the melting temperature.

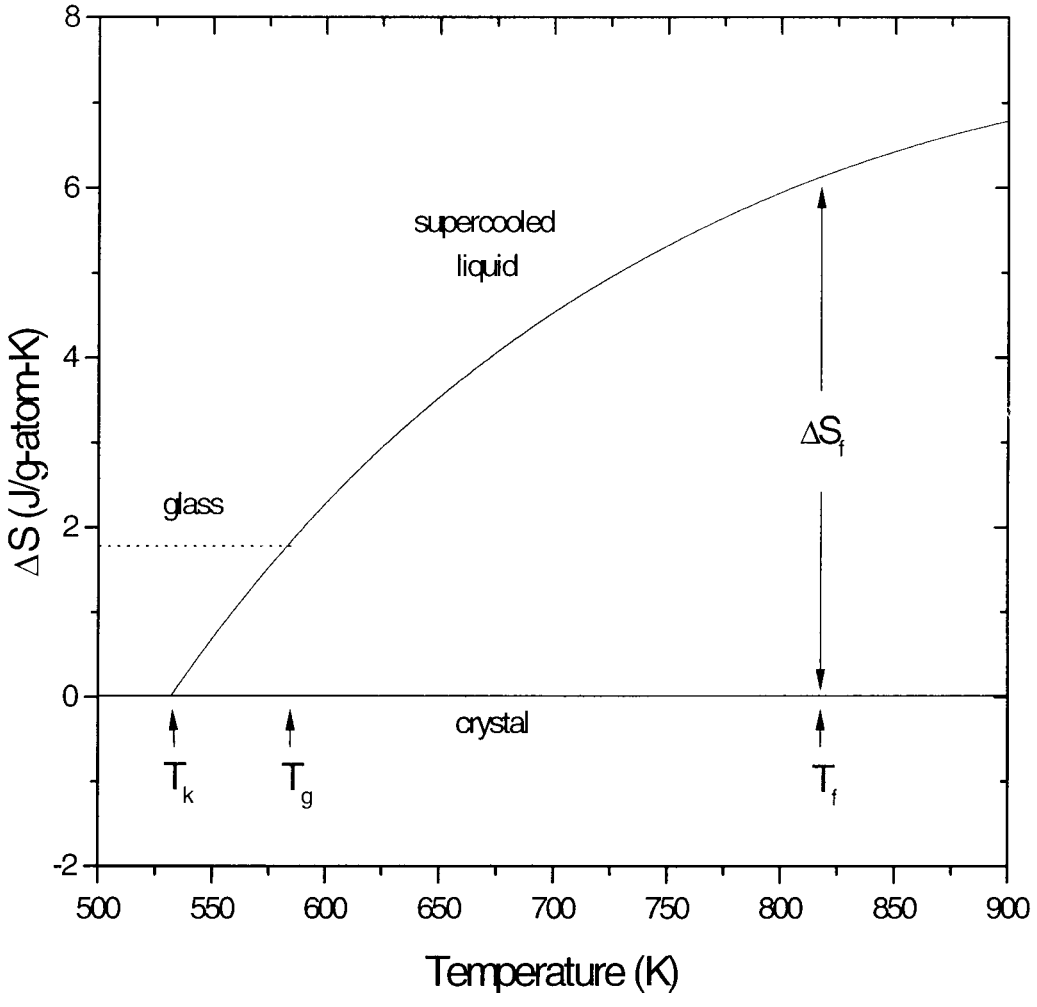

Figure 13: Entropy difference between the liquid and solid states of $Pd_{43}Ni_{10}Cu_{27}P_{20}$. T_k is the the Kauzmann temperature. T_g is the glass transition temperature. T_f is the melting temperature.

$$\Delta H^{l-x}(T) = \Delta H_f - \int_T^{T_f} \Delta c_p^{l-x}(T')dT' \tag{8}$$

where ΔH_f is the heat of fusion, and T_f is the temperature where Gibbs free energy of liquid and crystal are equal. Even though the melting temperature, T_m, can not be determined exactly, the peak of temperature, T_f, as defined in Figure 8 is normally a good approximation for T_f. In Figure 12, using equation (8), the enthalpy difference between liquid and crystalline state is shown. T_k is the Kauzmann temperature. T_g is the glass transition temperature. T_f is the melting temperature.

The difference in entropy between the crystal and liquid is defined by the heat of fusion and the temperature change of the specific heat capacity between liquid and crystal. The equation is given by

$$\Delta S^{l-x}(T) = \Delta S_f - \int_T^{T_f} \frac{\Delta c_p^{l-x}(T')}{T'} dT' \tag{9}$$

where ΔS_f is entropy of fusion, which is given by

$$\Delta S_f = \frac{\Delta H_f}{T_f} \tag{10}$$

There is residual entropy frozen into the glass below the transition temperature, as well as enthalpy. In Figure 13, using the equation (9), the entropy difference between liquid and crystalline state is shown.

It is important to note that the entropy difference calculated by heat of fusion and the heat capacity difference is not only configurational entropy difference but also vibrational entropy difference. This entropy difference would give us to know the Kauzmann temperature that a supercooled liquid cannot remain under this temperature

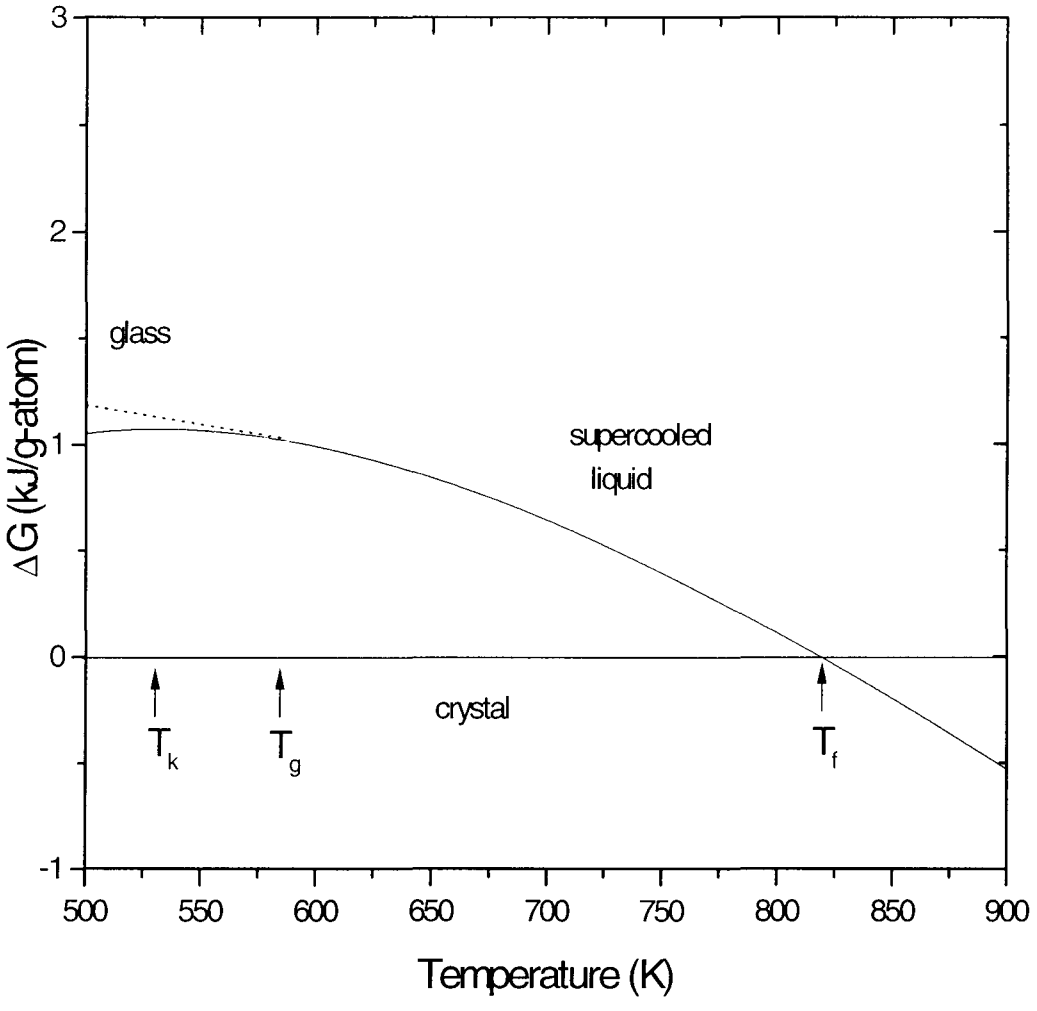

Figure14: The Gibbs free energy difference between the liquid and crystalline states of $Pd_{43}Ni_{10}Cu_{27}P_{20}$. T_k is the the Kauzmann temperature. T_g is the glass transition temperature. T_f is the melting temperature.

without either crystallizing or forming a glass so the Kauzmann temperature is the lowest possible temperature of the supercooled liquid state [16]. In addition, the Kauzmann temperature is the temperature at which configurational entropy of liquid is equal to entropy of crystal. The Kauzmann temperature might not be found at the temperature where configurational entropy of liquid and solid meet. The entropy increases with increase temperature, and it looks similar to shape of enthalpy difference of liquid and solid.

The calculation for the Gibbs free energy difference between liquid and crystalline state is given by

$$\Delta G^{l-x}(T) = \left(\Delta H_f - \int_T^{T_f} \Delta c_p^{l-x}(T')dT' \right) - T\left(\Delta S_f - \int_T^{T_f} \frac{\Delta c_p^{l-x}(T')}{T'} dT' \right) \qquad (11)$$

The specific heat capacity, enthalpy, and entropy were already calculated in the previous step.

The Gibbs free energy difference decreases with increasing temperature, and the free energy difference approaches zero when the temperature approaches the melting point. A difference of Gibbs free energy between liquid and crystalline state for the sample, $Pd_{43}Ni_{10}Cu_{27}P_{20}$, is shown in Figure 14 along with the estimated the critical cooling rate for this metallic glass-forming alloy. It can be seen that the driving force for crystallization is very small. The comparison to other metallic glass-forming alloys of the Gibbs free energy difference between liquid and crystalline state will be determined in the following chapter. This Gibbs free energy difference

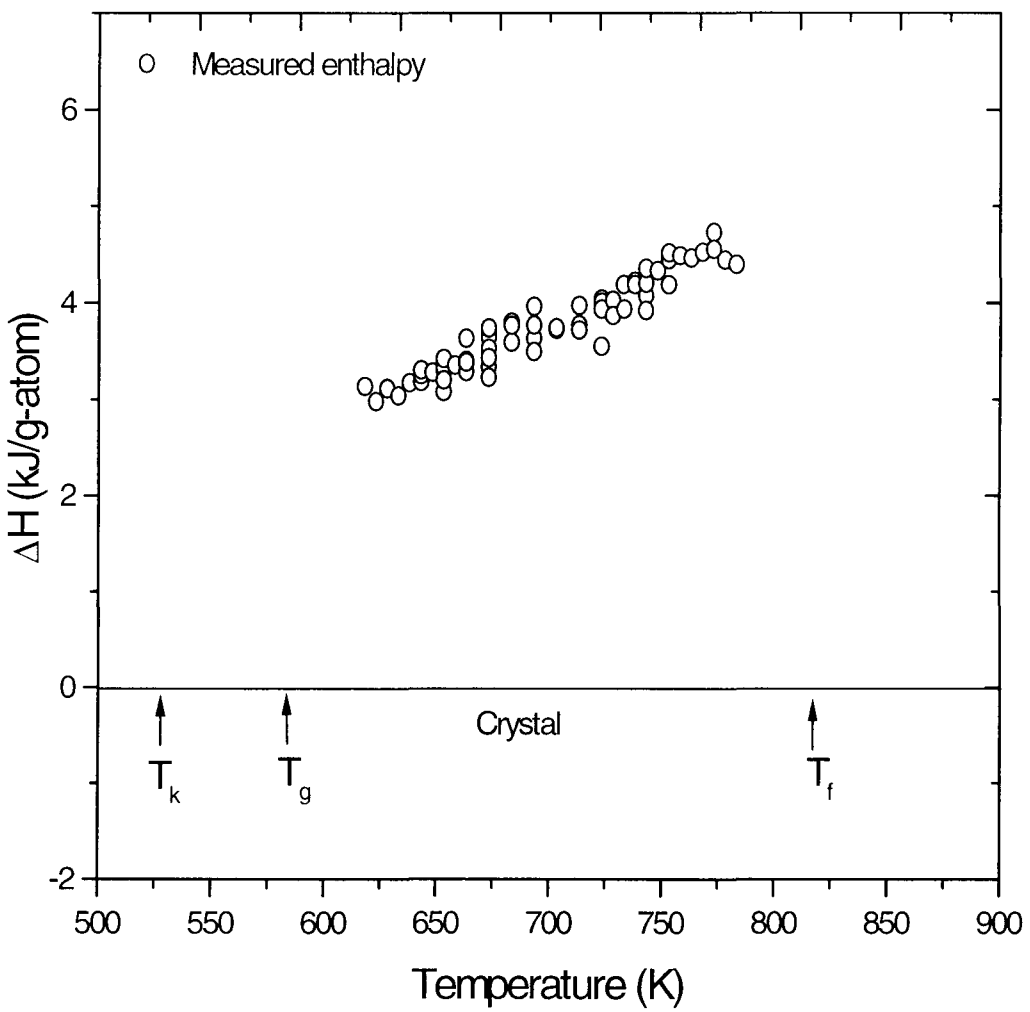

Figure15: Enthalpy difference between liquid and solid directly measured by DSC experiment.

between liquid and crystalline state is the driving force for crystallization only in the case of polymorphic transformation. This Gibbs free energy difference is the lower limit of the thermodynamic driving force for crystallization, unless the crystallization is polymorphic.

3.3 Direct Measurements of The Enthalpy Change During The Crystallization

The plot of the direct measurements of the enthalpy change during crystallization is shown in Figure 15. As it was shown in Figure 9, the heated sample above the melting temperature was cooled at certain temperatures, and was held long enough the isothermal crystallization completed. The measured temperature range was from 623 K to 783 K. The diagram shows that the enthalpy change decreases with decreasing temperature. The enthalpy change shifts from 3 to 5 kJ/g-atom in accordance with the specific heat capacity difference.

3.4 Time Temperature Transformation Diagram

To investigate the crystallization, the onset time of the crystallization temperature was measured. It was investigated that effect of fluxing the P-Ni-Cu alloy with B_2O_3 [12]. The results of effect of fluxing and no fluxing the $Pd_{43}Ni_{10}Cu_{27}P_{20}$ alloy are plotted in Figure 16. First, both fluxed and non-fluxed TTT diagram have the typical "C" shape to represent crystallization. The fluxed sample requires a longer

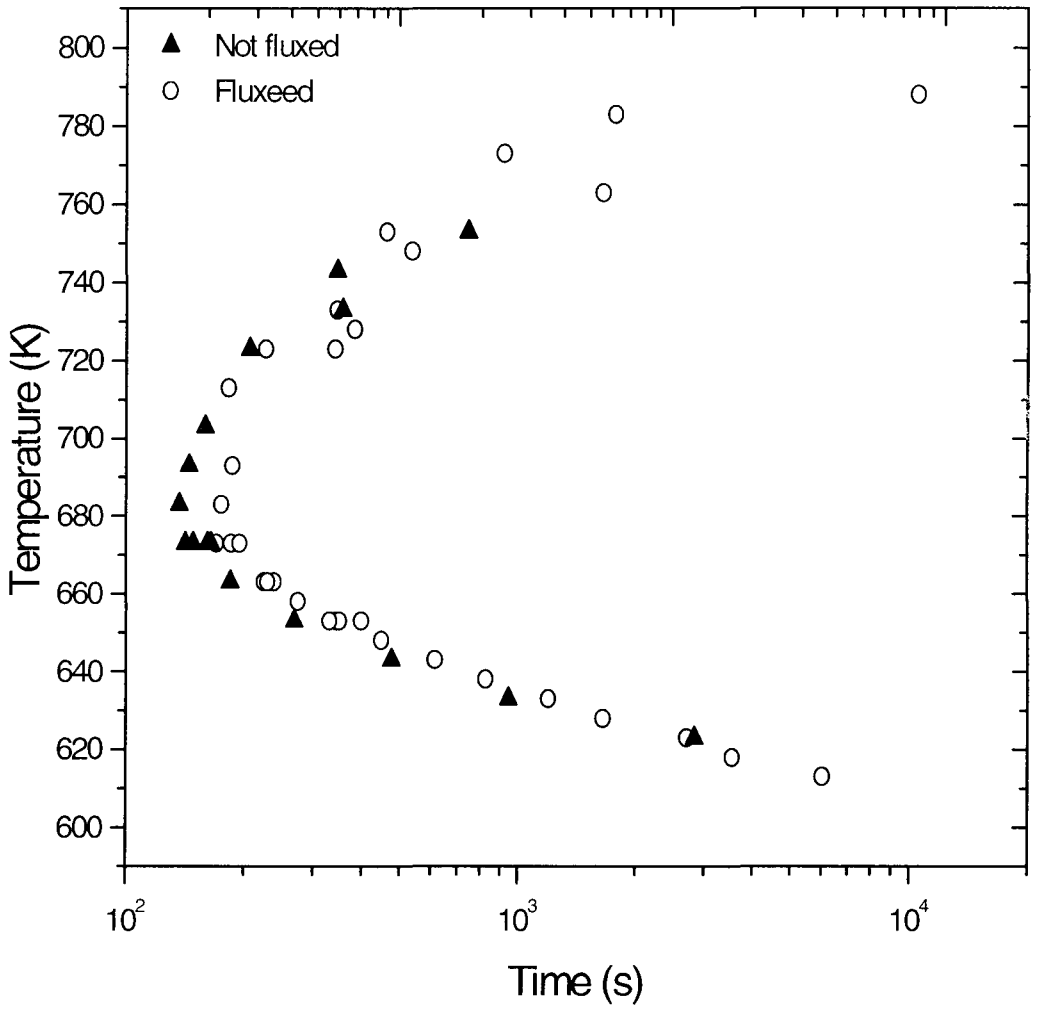

Figure 16: Time-temperature-transformation diagram of $Pd_{43}Ni_{10}Cu_{27}P_{20}$.

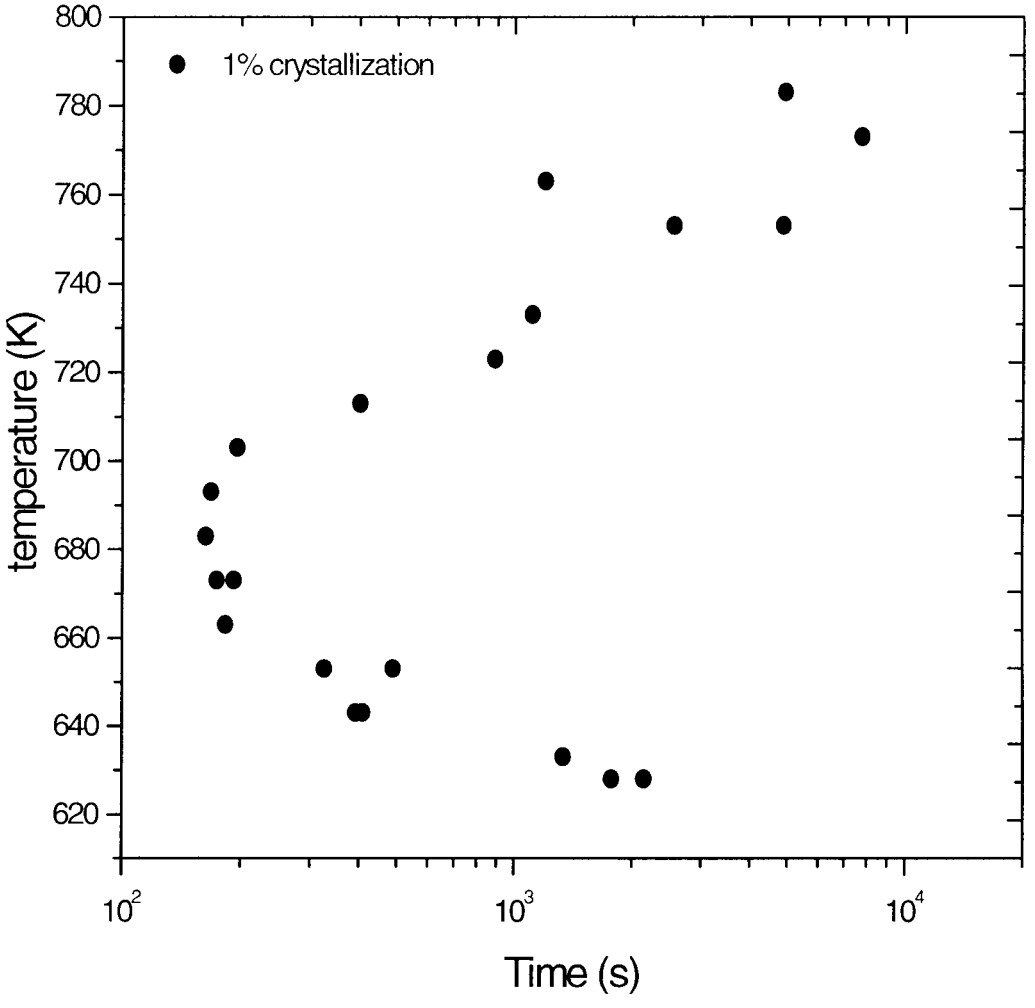

Figure 17: The time-temperature-transformation diagram of $Pd_{43}Ni_{10}Cu_{27}P_{20}$. The time to reach 1 % volume fraction is shown as a function of temperature.

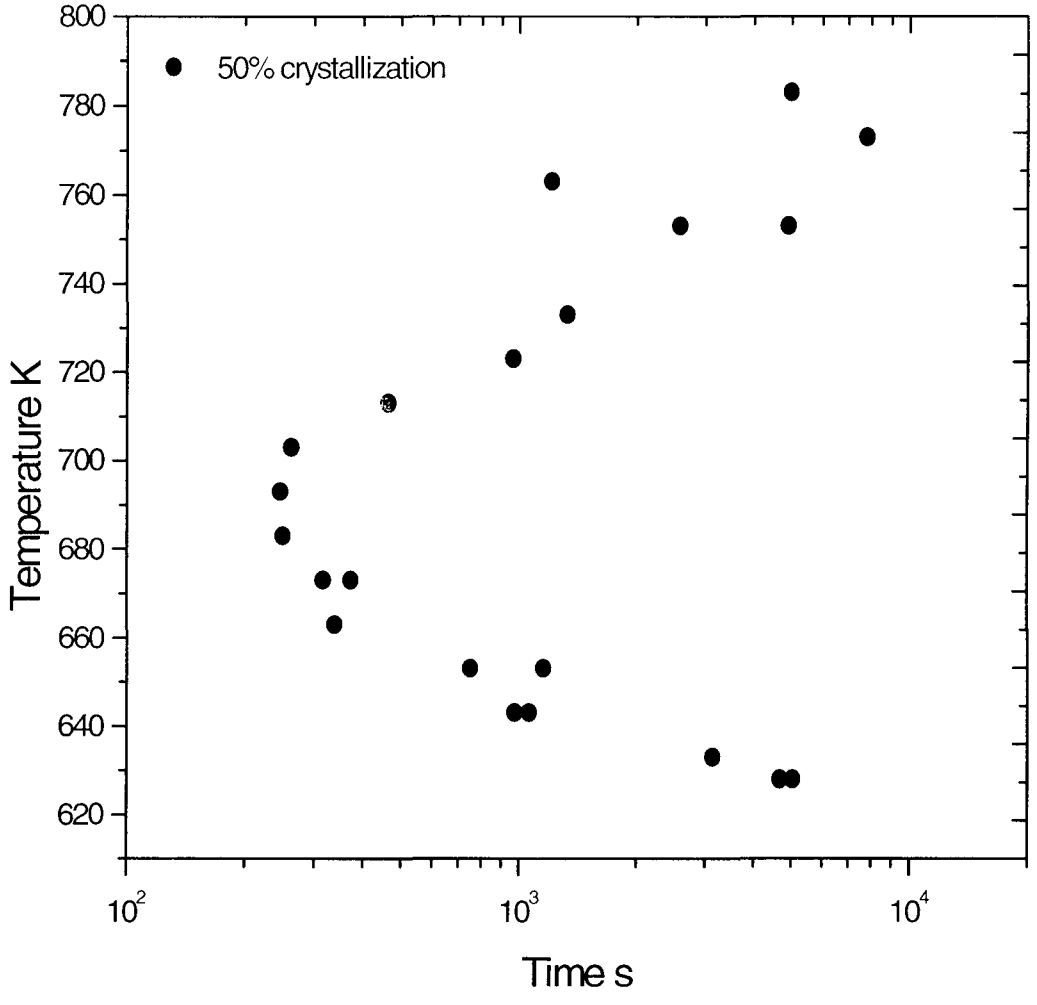

Figure 18: The time-temperature-transformation diagram of $Pd_{43}Ni_{10}Cu_{27}P_{20}$. The time to reach 50 % volume fraction is shown as a function of temperature.

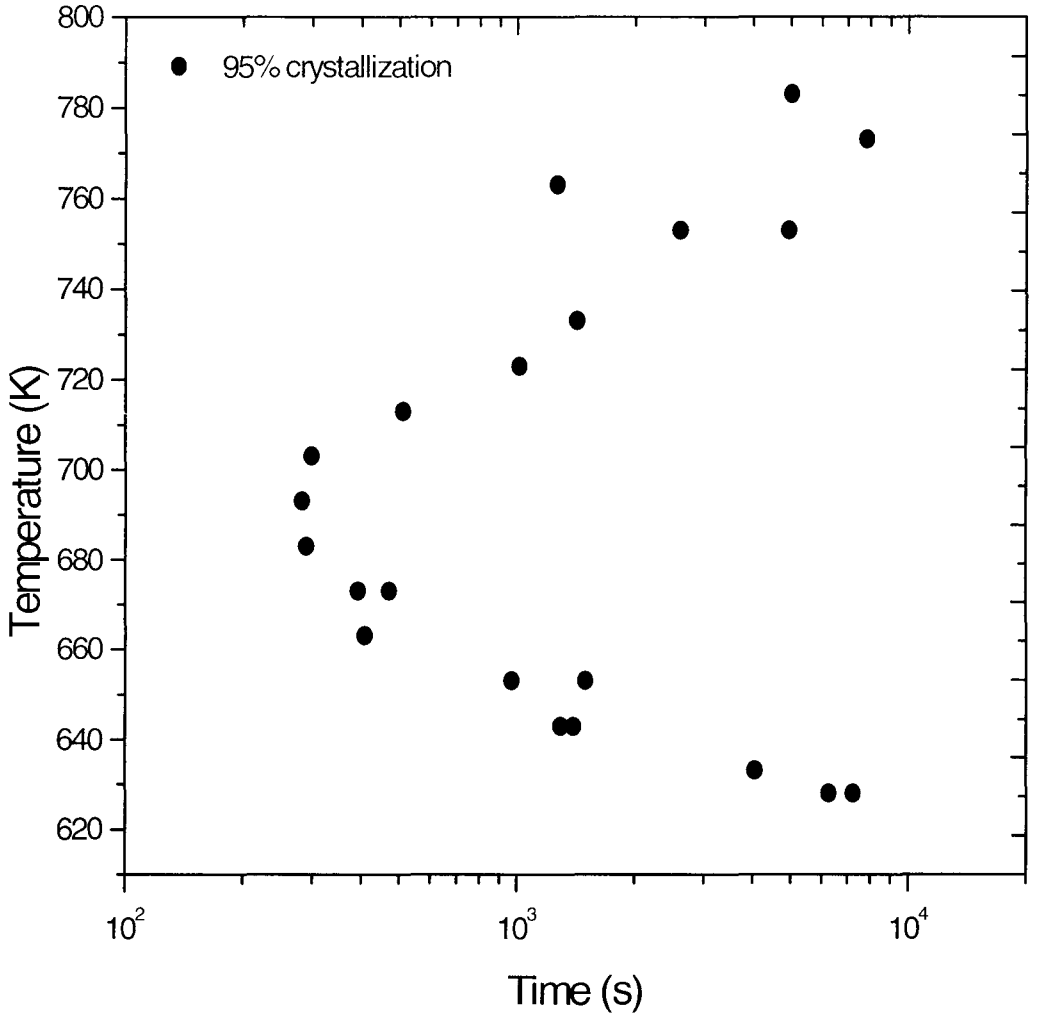

Figure 19: The time-temperature-transformation diagram of $Pd_{43}Ni_{10}Cu_{27}P_{20}$. The time to reach 95 % volume fraction is shown as a function of temperature.

time to start crystallization than non-fluxed samples. The nose, which defines the time and temperature where crystallization occurs the most rapidly, is at about 680 K and 125 s for non-fluxed sample, and is at about 680 K and 185 s for fluxed sample. The TTT curve of the fluxed sample shifts to the right for a few seconds from the TTT curve of non-fluxed sample. As a result of the TTT diagram, B_2O_3 fluxing enhances the sample's glass forming ability. Schroers [9] also investigated the effect of fluxing, and the result shown on the TTT curve of fluxed sample shifts to the right. Even though fluxed sample takes more time to be crystallized than the non-fluxed sample, even the non-fluxed samples have a good ability for vitrification.

The TTT diagram was constructed for 1 %, 50 %, and 95 % crystallized volume fraction to determine crystallization and growth rate for this sample, which is heat-treated. The growth of the crystallized volume fraction as a function of time was measured in the supercooled liquid regime under isothermal condition. Figure 17, 18, and 19 show the crystallization events. The time to reach 1% crystallization is 7200s at 773 K. It took only 90 s from 1 % of crystallization to 95 % of crystallization. The crystallization at 723 K was measured and its results were similar to the experiments at 773 K. Above 720 K, the time of crystallization from the beginning is first compared to the spent time at lower temperature. At 633 K, it took 1800 s to start crystallization, and 7000 s to complete crystallization. The experiments for 703 K show that 1% of crystallization occurred after 188 s, which took over 100 s since crystallization began, and fluxed and unfluxed samples presented very similar results

for 1 % crystallization. The difference between fluxed and unfluxed sample for crystallization is remarkable at temperature below nose of the diagram.

3.5 The Glass Transition and Crystallization Temperature Shift

The thermal behavior in the glass transition, the crystallization, and the melting of $Pd_{43}Ni_{10}Cu_{27}P_{20}$ is shown in Figure 20, and heating rate is 0.333 K/s. It displays the endothermal heat effect due to the glass transition, several steps of heat release during the crystallization events from metastable undercooled liquid state into the crystalline compounds at T_x = 669 K and subsequent temperature, and the melting transition. The crystallized sample reaches the melting region and starts to melt at the eutectic temperature, T_{eut} = 804 K. The peak of the melting event is recognized as melting temperature at the liquid temperature, T_{liq} = 818 K. The onset temperatures of the glass transition, T_g, and the crystallization temperature, T_x, are strongly dependent on the heating rate. The heat of fusion determined by integrating the peak area is also dependent on heating rate, but it is not as much as glass transition temperature and crystallization temperature are. In Figure 21, the glass transition temperature shifts for annealed sample are represented respect to the heating rate. In this experiments, two different glass transition temperatures, T_{g1} and T_{g2}, appear when the heating rate is faster than 1.333 K/s. The glass transition shift for non-annealed samples is presented in Figure 22. There is only one T_g observed in the non-pre annealed sample. The typical scan that shows two glass transition temperatures in the DSC is shown in

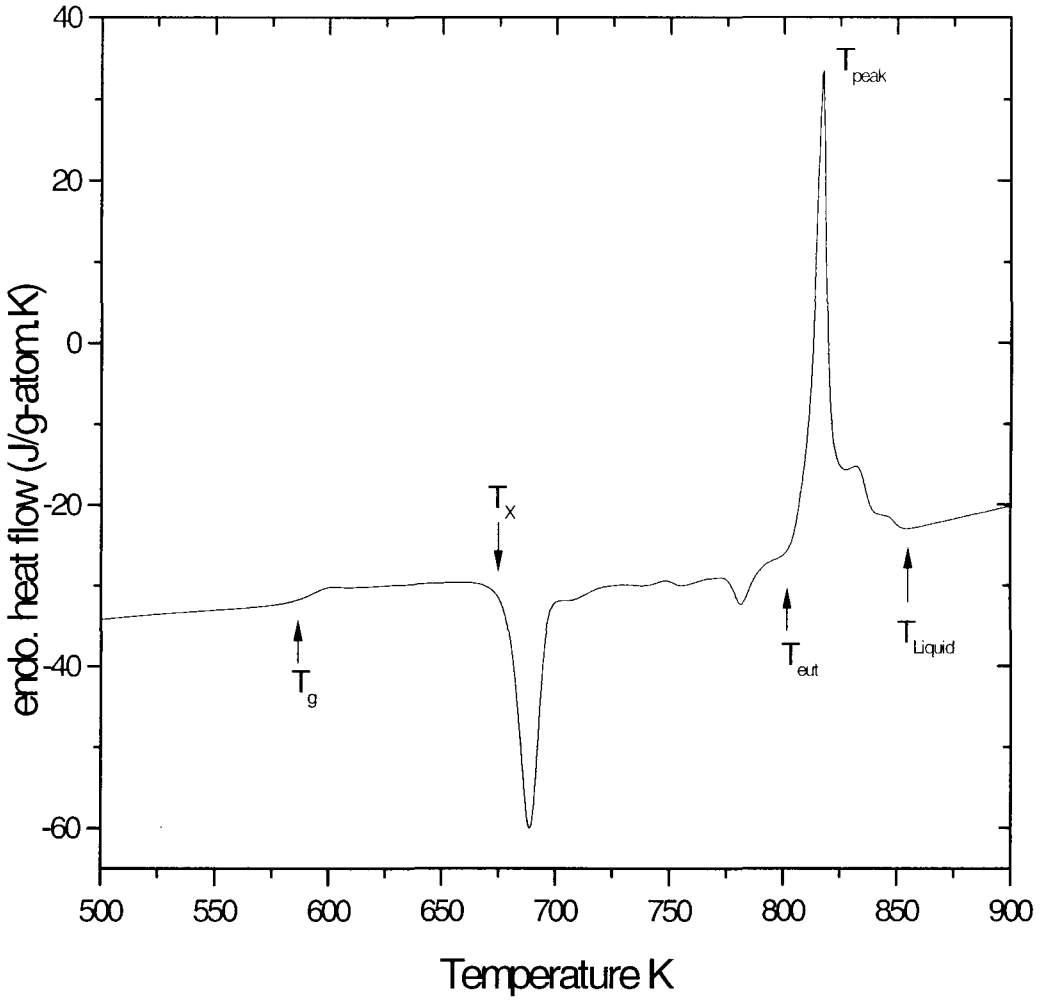

Figure 20: Thermal behavior of $Pd_{43}Ni_{10}Cu_{27}P_{20}$ upon heating. The plot is scanned by a DSC (Heating rate is 0.333K/s). T_g is the glass transition temperature, T_x is the crystallization temperature, T_{eut} is the solidus temperature, T_{peak} is the peak temperature of fusion, and T_{liquid} is the liquidus temperature.

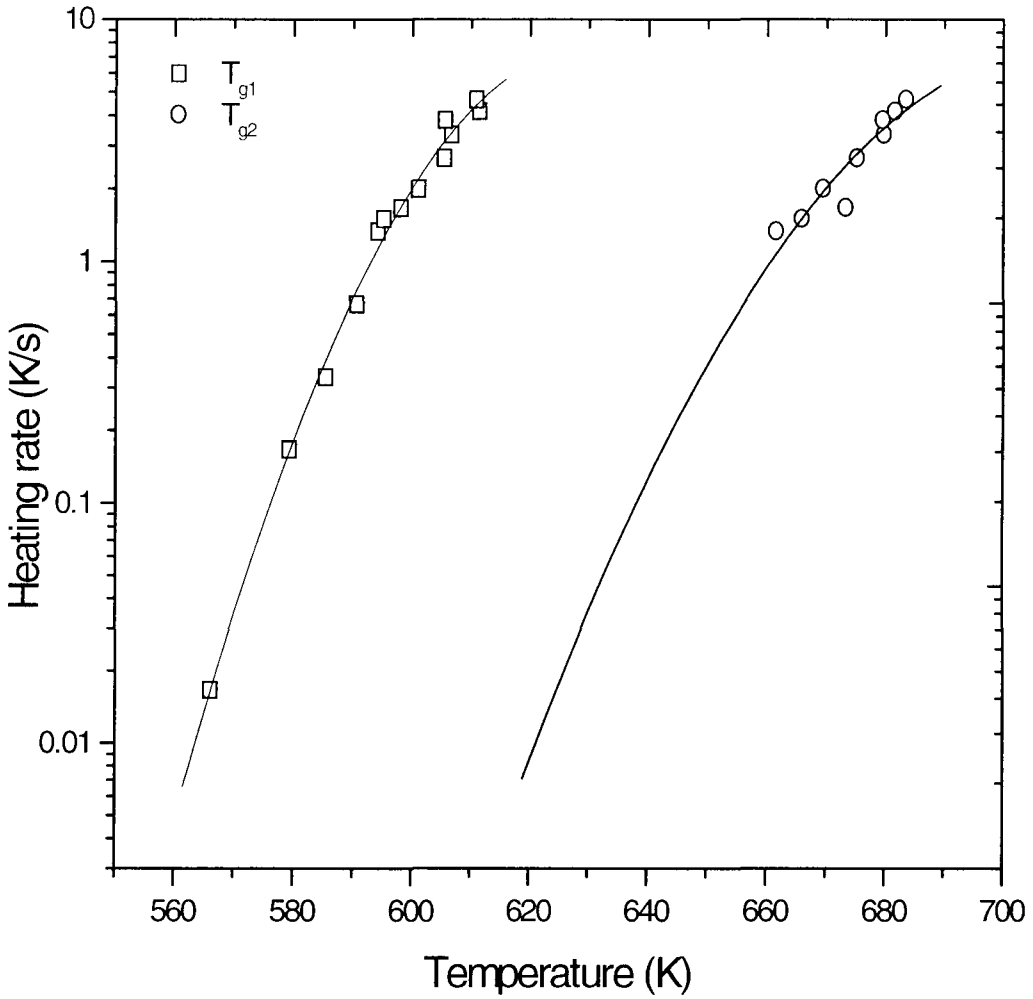

Figure 21: The glass transition temperatures as a function of the heating rate.

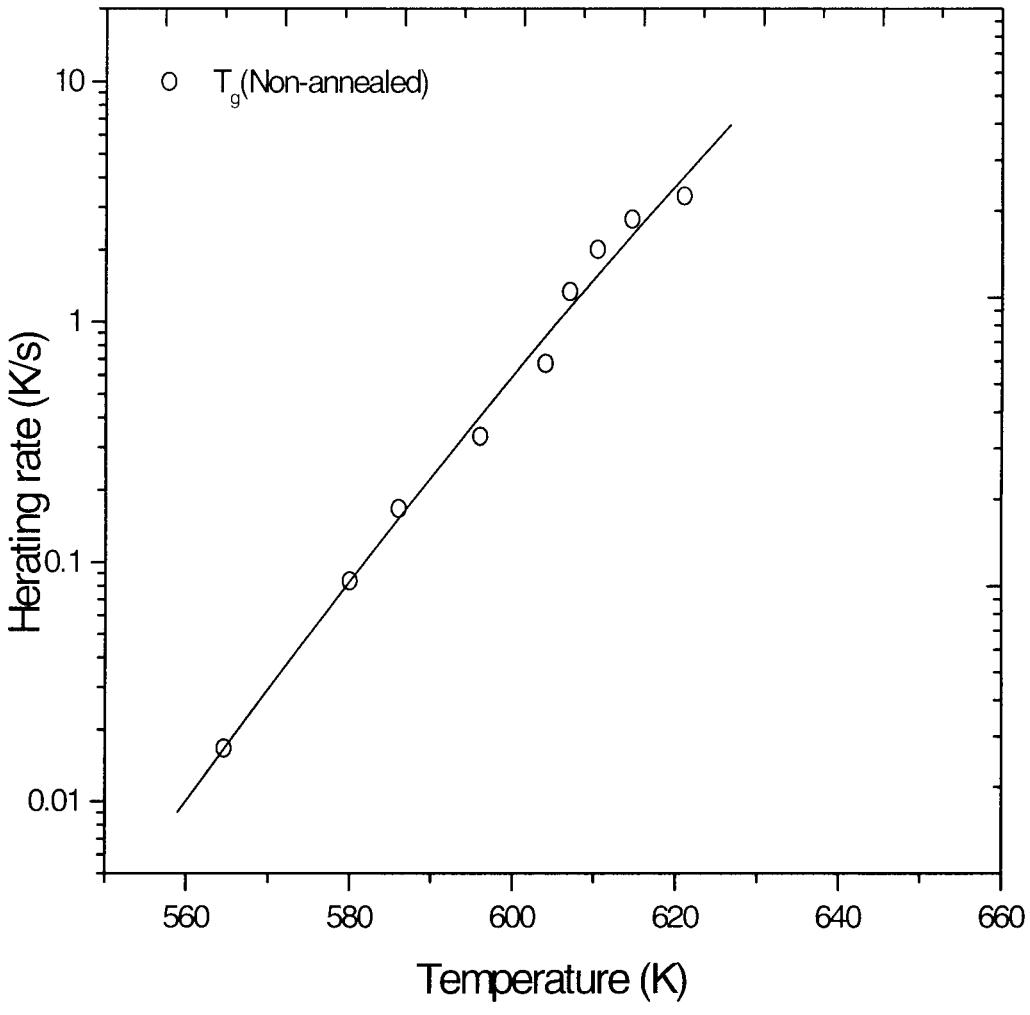

Figure 22: The glass transition temperature with respect to the heating rate. The plots show the glass transition temperature for non-annealed samples with several heating rate from 0.017 K/s to 5 K/s.

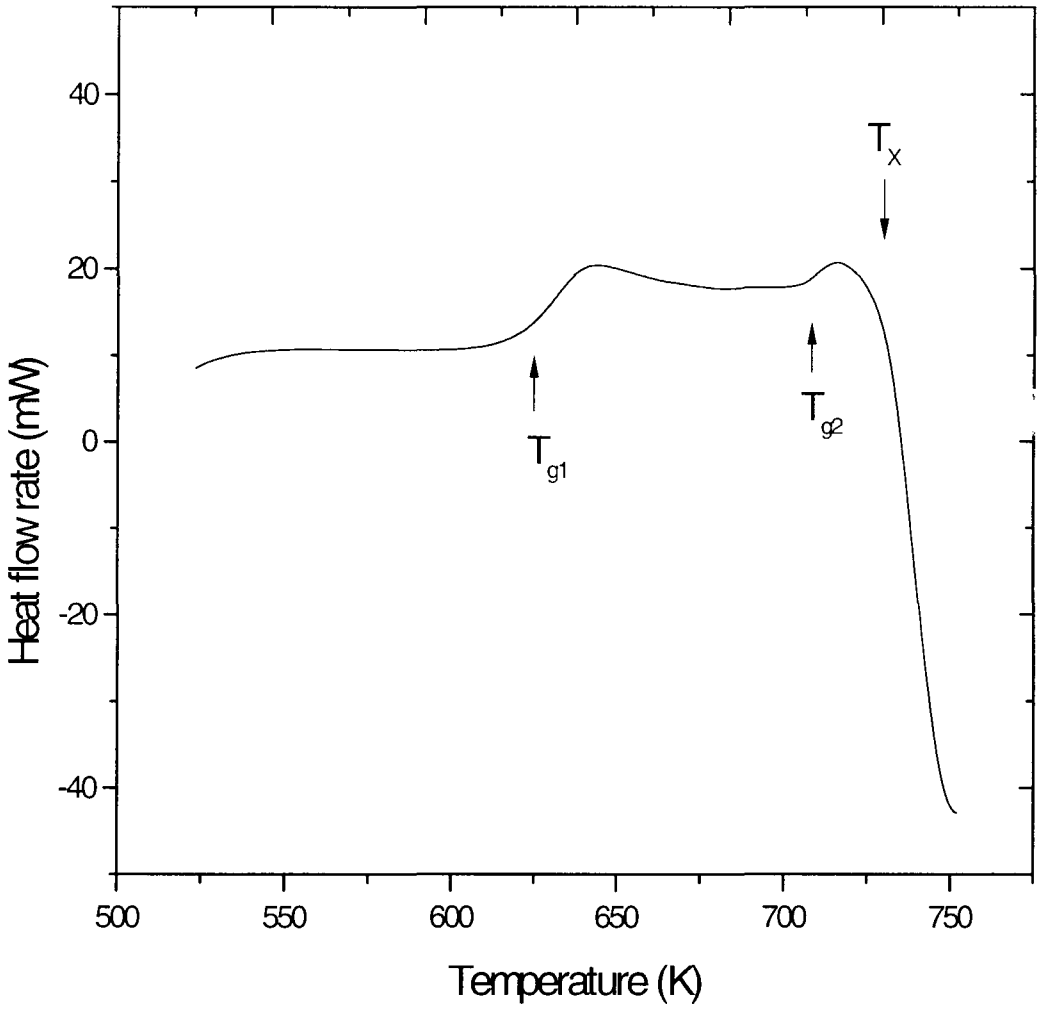

Figure 23: Typical DSC scanning from the undercooled liquid to the crystallization region at heating rate of 2.666 K/s for $Pd_{43}Ni_{10}Cu_{27}P_{20}$. The onset of both peaks is recognized as glass transition temperature.

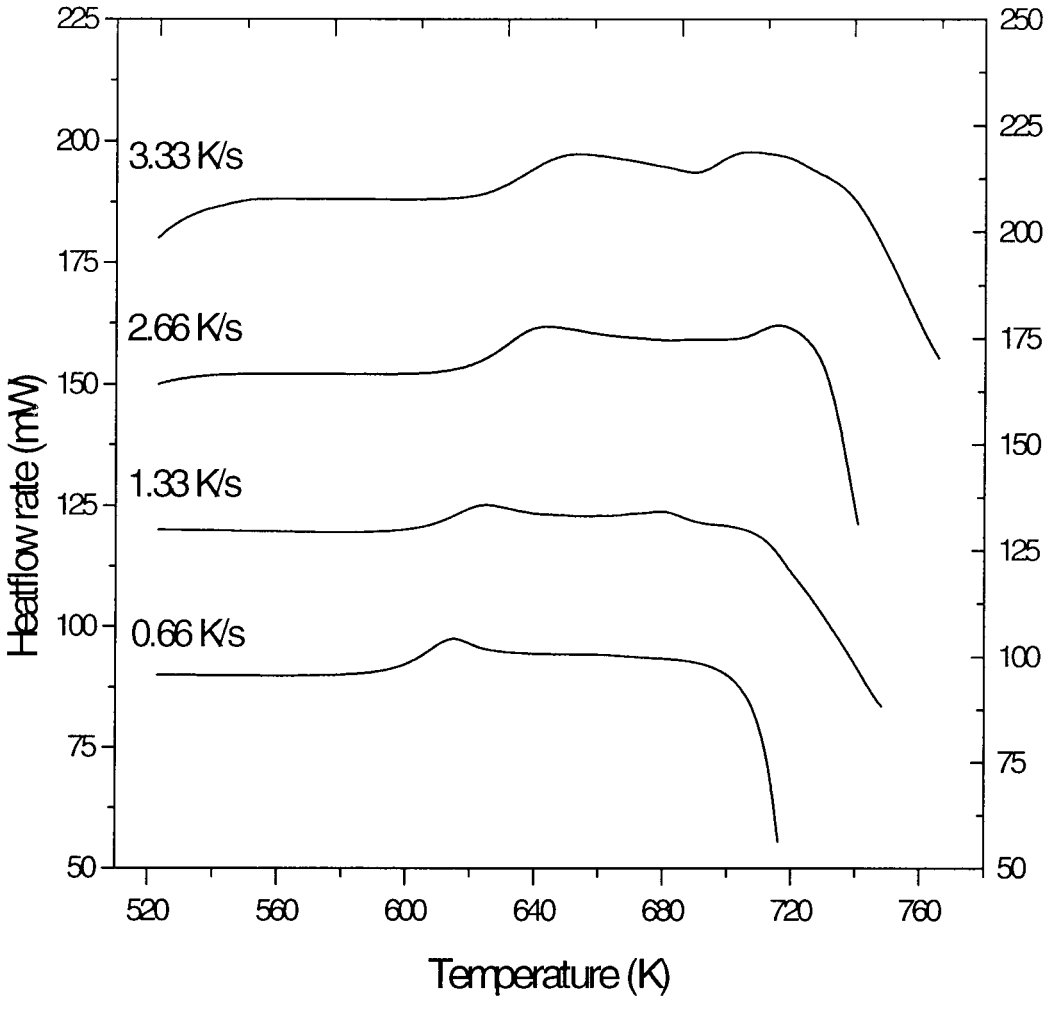

Figure 24: DSC scanning from undercooled liquid to the beginning of the crystallization region. Four line plots show the glass transition shifts.

Figure 23. Both glass transition temperatures are strongly heating rate dependent. The second glass transition temperature is observed in the heating rate range between 1.333 K/s and 4.666 K/s. At over 4.666 K/s heating rate, only one glass transition temperature exists in the experiment. The difference between T_{g1} and T_{g2} is about 75 to 85 K for any heating rate in that region. The glass transition temperature shift with different heating rate is shown in Figure 24.

3.6 Vogel-Fulcher-Tamann Expression

By the result of scanning the thermodynamic events through the undercooled liquid state to the crystalline state, the fragility of metallic glass-forming alloy can be determined. The inverse heating rate is plotted as a function of onset temperature of the glass transition in Figure 25. The total relaxation time can be determined normalized to $T_g^{'}$ which is usually close to T_g^* with the Vogel-Fulcher-Tamann-type equation, [17][18]

$$\tau_{T_g}^{tot}(T^*) = \tau_0 \cdot \exp\left(\frac{D^* \cdot T_0}{T^* - T_0}\right) \tag{12}$$

Where $\tau_{T_g}^{tot}$ is the total relaxation time, τ_0 is inversed heating rate, D^* is the fragility parameter, and T_0 is the VFT temperature. The fragility parameter is used for classifying the different temperature dependence of the viscosity [19][20]. The fragility parameter and VFT temperatures are in excellent agreement with the values obtained from fitting the relaxation the glass transition using the shift of the onset of

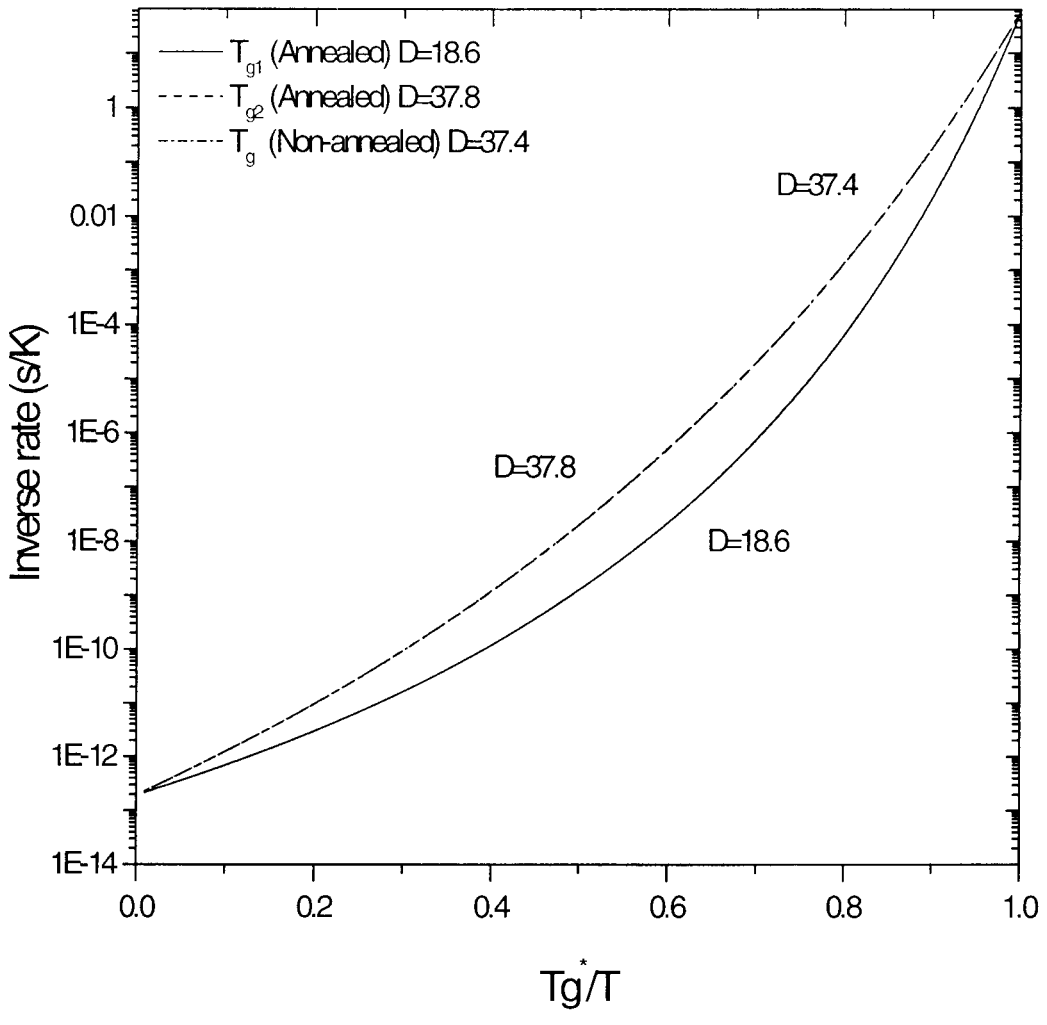

Figure 25: Overall picture: Inverse heating rate as a function of onset temperature of the glass transition measured with a rate of 0.333 K/s. The data were fitted with a VFT-type equation.

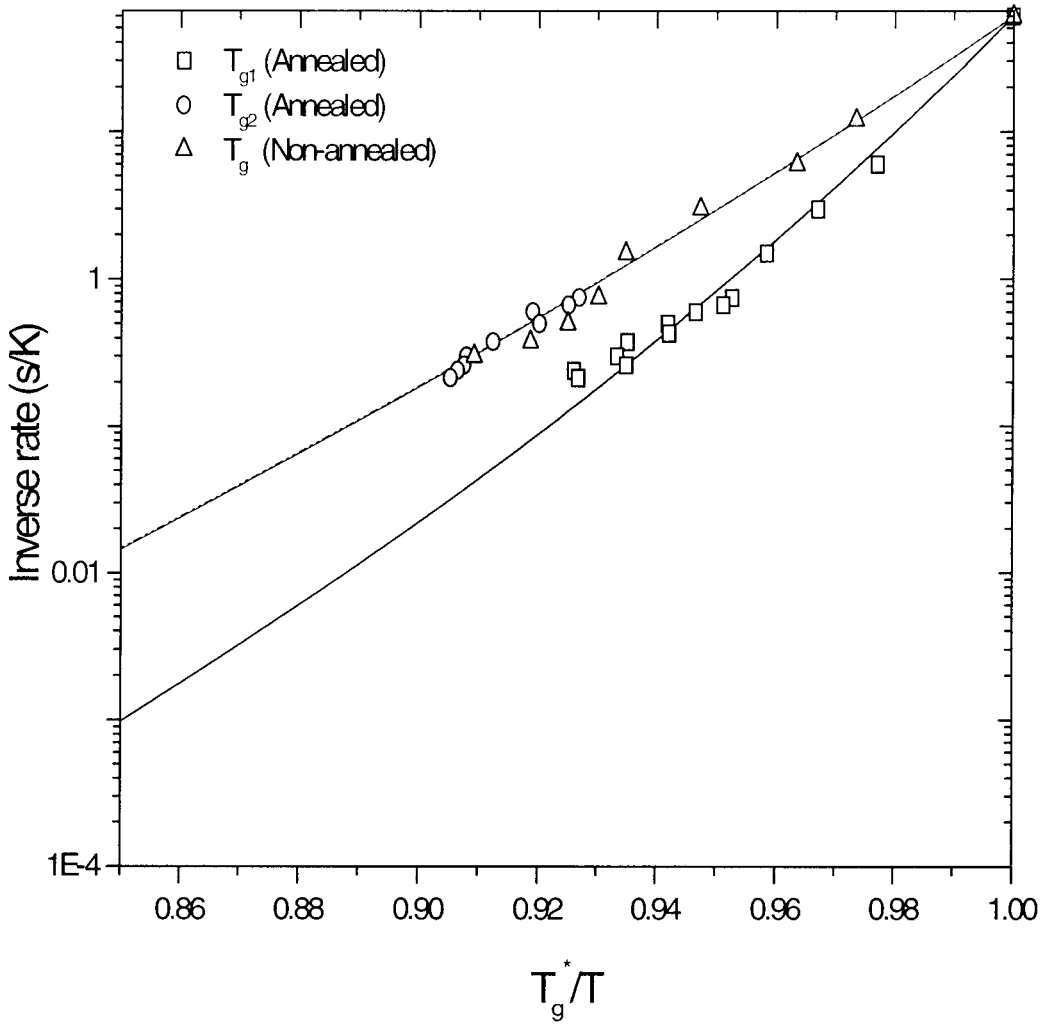

Figure 26: Specified picture: Inverse heating rate as a function of onset temperature of the glass transition measured with a rate of 0.333 K/s. Annealed sample and the first glass transition temperature (square), Annealed sample and the second glass transition temperature (circle), and non-annealed sample and the glass transition temperature (triangle). The data were fitted with a VFT-type equation.

T_g with heating rate. The heating rate dependence of the onset of T_g can be parameter as a measure for the fragility of the glass, even if the supercooled liquid is experimentally not accessible. For the all T_g, τ_0 is 1.9216×10^{-13} s/K. The parameter for T_{g1} of annealed sample, D^* is 18.6, and T_0 is 363.48. For T_{g2} of annealed sample, D^* is 37.8, and T_0 is 289.21. For T_{g1} of non-annealed sample, D^* is 37.4, and T_0 is 226.44. The rapid increase of the relaxation kinetics with rising temperature reduces its thermal stability with respect to crystallization. As it can be seen from the plots, two different glass regions in the sample, which has different glass transition temperature, have different fragilities. The second glass transition temperature fit shows higher fragility than first glass transition temperature fit. The T_{g1} has fragility parameter as 18.6, and T_{g2} has 37.4. In the Figure 26 non-annealed sample is plotted, and it has very similar curve and fragility. The fragility parameter of non-annealed sample is 37.8.

4. DISCUSSION

The specific heat capacity of $Pd_{43}Ni_{10}Cu_{27}P_{20}$ alloy was measured with respect to a sapphire standard for amorphous solid, crystalline solid, supercooled liquid, liquid state, and the diagram of them was shown in Figure 11.

By determining the free energy difference between liquid state and crystalline state, a measurement for the glass forming ability can be found. In general, the bigger the free energy differences between crystalline and liquid state, the smaller the glass forming ability of the alloys. It is important to note that this free energy difference between crystalline and liquid state is the driving force for the crystallization only for a polymorphic transformation situation. In other words, this free energy difference between them is the lower limit of thermodynamic driving force for crystallization, unless that crystallization is polymorphic. As a general definition, the metallic glass-forming alloys, which have excellent glass forming ability, must have the smaller entropy of fusion.

The table 1 shows the enthalpy of fusion, the entropy of fusion, the melting temperature, the glass transition temperature, and the Kauzmann temperature. All data were from Figure 12, 13, and 14. The T_k is the Kauzmann temperature. The Kauzmann temperature is the isentropic temperature, the temperature at which the entropy of liquid is equal to the entropy of crystal (See Figure 13). Because the difference of the enthalpy and entropy between liquid and crystalline state were small, the difference in the Gibbs free energy has been very small. The smaller difference of

	ΔH_f (kJ g atom^{-1})	ΔS_f (J g atom^{-1})	T_m (K)	T_g (K)	T_K (K)
$Pd_{43}Ni_{10}Cu_{27}P_{20}$	5.0185	6.134	818.2	585.4	531

Table1: Enthalpy difference, entropy difference, melting temperature, glass transition temperature, and Kauzmann temperature for the metallic glass forming alloy, $Pd_{43}Ni_{10}Cu_{27}P_{20}$.

Gibbs free energy between liquid and crystalline states, the greater is the ability of vitrification for metallic glass-forming alloy. Figure 27 represents the free energy difference for several metallic glass-forming alloys including the $Pd_{43}Ni_{10}Cu_{27}P_{20}$ alloy [13][21][22]. It is significant that the sample has a very small free energy difference compared to other amorphous alloys.

To define whether the sample alloy has an excellent glass forming ability, there is another parameter, T_{rg}, [23] which is termed the reduced glass transition temperature. This T_{rg} is given by

$$T_{rg} = \frac{T_g}{T_m} \tag{14}$$

where T_g is the glass transition temperature, and T_m is the melting temperature. This idea was developed by Turnbull in his theory of nucleation and growth of the

crystalline state from an undercooled liquid [23]. The glass transition temperature can be measured by DSC scan. Figure 8 shows the glass transition temperature, T_g and crystallization temperature, T_x. The bigger the reduced glass transition temperature, T_{rg}, the better is glass forming ability. In this study, the $Pd_{43}Ni_{10}Cu_{27}P_{20}$ alloy has a T_{rg} of 0.71.

Sample name	Critical cooling rate (K/s)	T_{rg}
$Pd_{43}Ni_{10}Cu_{27}P_{20}$	0.09	0.71
$Zr_{41.2}Ti_{13.8}Cu_{12.5}Ni_{10}Be_{22.5}$	1	0.67
$Zr_{57}Cu_{15.4}Ni_{12.6}Al_{10}Nb_5$	10	0.62
$Zr_{52.5}Cu_{17.9}Ni_{14.6}Al_{10}Ti_5$	10	0.62
$Mg_{65}Cu_{25}Y_{10}$	50	0.59
$Cu_{47}Ti_{34}Zr_{11}Ni_8$	1000	0.60

Table 2: Critical cooling rates and reduced glass transition temperature of selected metallic glass alloys.

Table 2 shows T_{rg} and critical cooling rate for some metallic glass-forming alloys including the $Pd_{43}Ni_{10}Cu_{27}P_{20}$ alloy with their critical cooling rate[23][24][25][26][27].

The glass forming ability for this alloy has been evaluated by calculated enthalpy, entropy, and Gibbs free energy difference between liquid state and

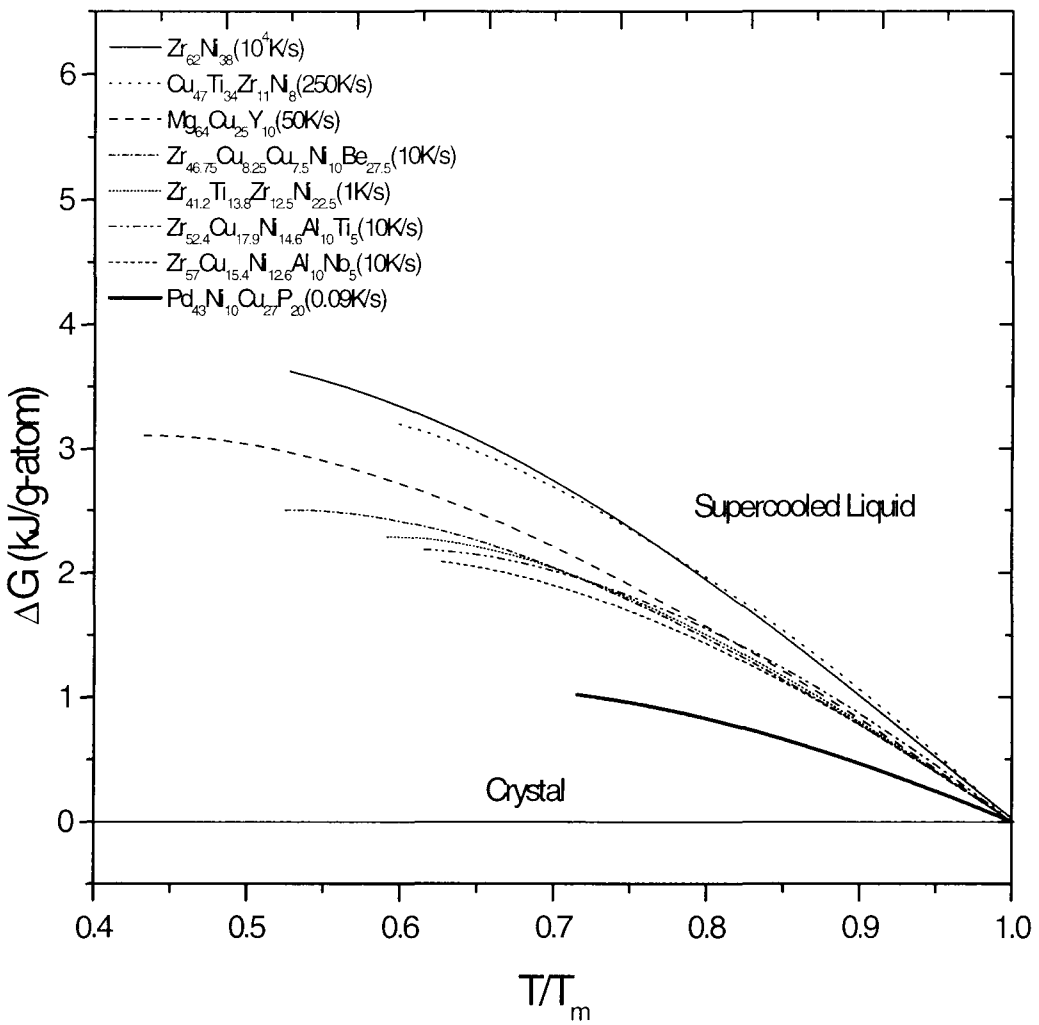

Figure 27: The Gibbs free energy difference between the liquid and crystalline states for a number of metallic glass-forming alloys. These data have been normalized by melting temperatures of the alloys. Also listed for these alloys is the critical cooling rate of glass formation. Data of other alloys were taken from reference [13][21][22].

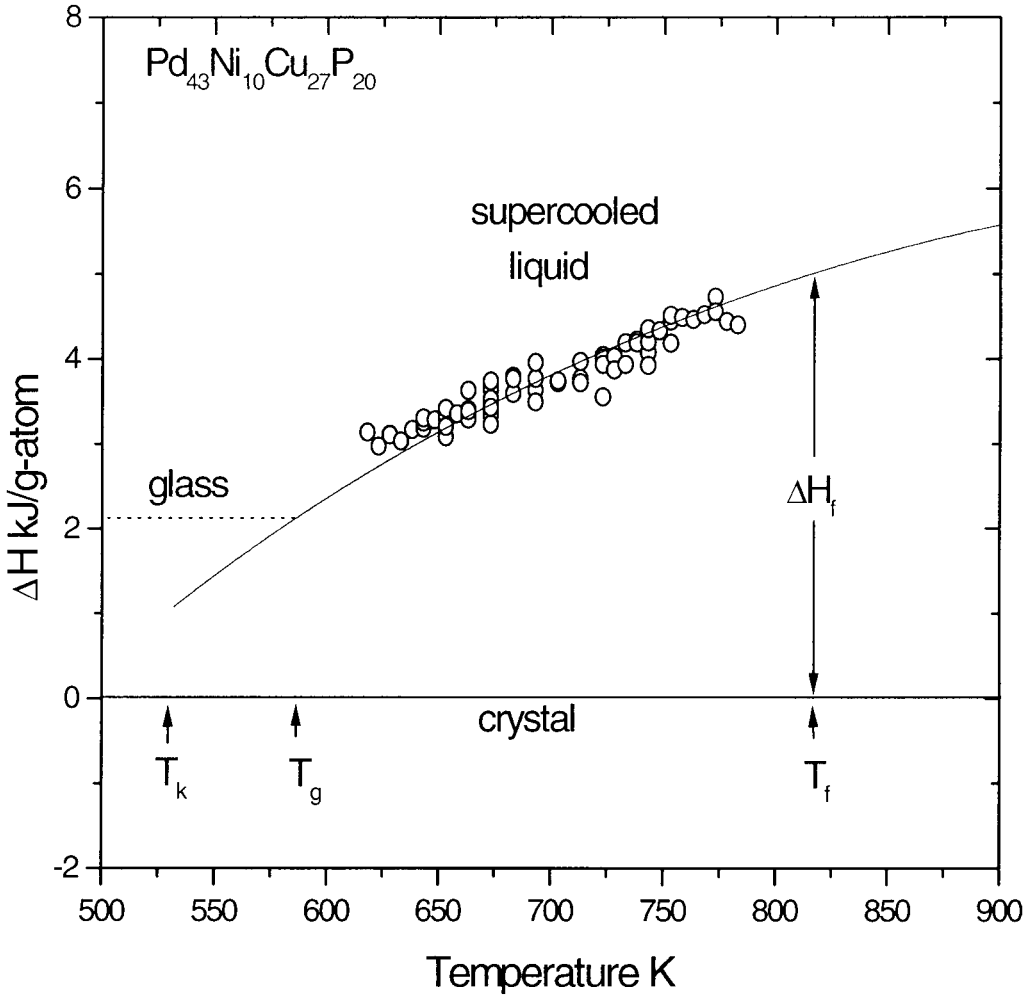

Figure 28: Enthalpy difference between the liquid and solid of $Pd_{43}Ni_{10}Cu_{27}P_{20}$. The circles represent enthalpy difference between liquid directly measured from DSC experiment. T_k is the Kauzmann temperature. T_g is the glass transition temperature. T_f is the melting temperature.

crystalline state. In general, the smaller the driving force, the better is the glass-forming ability of the metallic alloy. As it is shown in Figure 14, the Gibbs free energy difference between liquid and crystalline state in this alloy was very small. T_g/T_m in the table also shows the high ability of glass formation for these alloys. From enthalpy calculation and scanning of exothermic reaction of sample up to 850 K, the Kauzmann temperature, glass transition temperature, and melting temperature were determined. The reliability of this calorimetric experiment is proved by Figure 28. The line plot based on mathematical data and the plots as circle based on direct measurement from experiments under isothermal condition exactly matches each other. As a result, the data of the specific heat capacity can be considered highly accurate and reliable.

From the TTT diagram, it is also evident that the $Pd_{43}Ni_{10}Cu_{27}P_{20}$ alloy is better metallic glass-forming alloy than others. The crystallized volume fraction in the isothermal experiment with steady state nucleation rate is described by

$$x(t) = 1 - \exp\left[-\frac{\pi}{3}u^3 I_{ss} t^4\right] \tag{14}$$

I_{ss} indicates the nucleation rate, which is given by

$$I_{ss}(t) = \frac{A_v}{\eta(t)} \exp\left[-\frac{16\pi\sigma^3}{3k_B T \Delta G(T^2)}\right] \tag{15}$$

where A_v is a constant of the order of 10^{32} Pas/m^{3}s, η is the viscosity, ΔG is the difference in Gibbs free energy, k_B is the Boltzman constant, and σ is the energy of the interface between nuclei and liquid. The temperature dependence of the viscosity

of the Pd-based alloys can be described by a Vogel-Fulcher-Taman expression, [17][18]

$$\eta = \eta_0 \exp\left(\frac{D^* \cdot T_0}{T - T_0}\right) \tag{16}$$

where η_0=4*10^{-5} Pas, the fragility parameter, D^* = 18.6, and T_0 = 404 K. The temperature dependence of ΔG can be determined by Turnbull's linear expression, which is given by

$$\Delta G = \Delta S_f \left(T_{liq} - T\right) \tag{17}$$

where ΔS_f = 8.03 J/K-mol and T_{liq} = 873 K. The growth rate of diffusion is described by

$$u = \frac{D}{(2Dt)^{\frac{1}{2}}} \tag{18}$$

where D is the diffusivity. The beginning of the crystallization can be determined by

$$x(t) = \frac{\pi}{3Iut^4} \tag{19}$$

It is assumed that the nucleation rate at 753 K is 10^4 nuclei/s-m^3 for a fit of the nucleation rate since one nuclei formed after 1000 s in the sample. The temperature dependence of the diffusivity was determined by the Stokes-Einstein equation

$$D = \frac{k_B T}{3\pi\eta a} \tag{20}$$

where a is an average atomic distance, and it is 3.1×10^{-8}. The fit gives an interfacial energy of 79 mJ and A_v = 1×10^{30} Pas/m^{3}s. It is assumed that growth rate u is a

constant value taken at $t_{50\%}$. The rate of the crystallization can be determined by differentiating equation (14), which is given by

$$\frac{dx(t)}{dt} = \frac{4\pi}{3} u^3 It^3 \exp\left[-\frac{\pi}{3} u^3 I_{ss} t^4\right] \tag{21}$$

$$\frac{dx(t)}{dt} = \pi u^3 Nt^2 \exp\left[-\frac{\pi}{3} u^3 Nt^3\right] \tag{22}$$

The crystallization event was calculated with equation (22). The crystallization rate and growth rate are shown in Table 3.

After the sample was annealed at 733 K, with heating rate of 0.333 K/s, exothermal reaction under isothermal condition was observed by DSC. That

Temperature (K)	Crystallization rate ($1/m^3s$)	Growth rate (m/s)
623	1×10^{17}	1.6×10^{-12}
703	1×10^{16}	3.6×10^{-10}
723	1×10^{14}	7×10^{-10}
773	1×10^{5}	3×10^{-9}

Table 3: The crystallization and growth rate at certain temperature.

observation scanned all events including the glass transition, crystallization, and melt. At higher than 1.333 K/s heating rate, more than one glass transition temperature was observed before it was crystallized during experiment. Because of annealing, the phase was decomposed into the solute and solvent amorphous phase. By each glass transition temperature shift, the parameter of fragility can be determined with Vogel-Fulcher-Tamman equation. When the glass transition temperature is fitted with the VFT equation, the strong liquid has high fragility parameter up to 100 and the fragile liquid has low fragility parameter as low as 2. As it can be seen in Figure 25, and 26, annealed sample has two different fragilities, $D^* = 18.6$, $D^* = 37.8$, and non-annealed sample has fragility parameter, $D^* = 37.4$. Those results are also evidence for decomposition of the sample by annealing. The fragility parameters of several metallic glass forming alloys are compared in Table 4 [28][29]. The larger fragility parameter means that alloy has better glass-forming ability. The metallic glass-forming alloy, which has a large fragility parameter, has sluggish kinetics in the supercooled liquid regime and inhibits crystallization. Table 4 shows that the sample, $Pd_{43}Ni_{10}Cu_{27}P_{20}$, has high ability of glass formation. The fragility parameter of this sample is much higher than other metallic glass-forming alloys.

Sample	critical cooling rate (K/s)	D^*	D^*
$Pd_{43}Ni_{10}Cu_{27}P_{20}$ (annealed)	0.09	18.6	37.8
$Pd_{43}Ni_{10}Cu_{27}P_{20}$ (non-annealed)	0.09	37.4	
$Zr_{46.75}Ti_{8.25}Cu_{7.5}Ni_{10}Be_{27.25}$	18	22.7	
$Zr_{41.2}Ti_{13.8}Cu_{12.8}Ni_{10}Be_{22.5}$	1	18.5	
$Pd_{48}Ni_{32}P_{20}$	<10	16.6	
$Cu_{47}Ti_{34}Zr_{11}Ni_8$	1000	12.0	
$Pd_{77.5}Cu_6Si_{16.5}$	500	11.1	
$Au_{77.8}Ge_{13.8}Si_{8.4}$	$\sim 10^5$	8.4	

Table 4: Critical cooling rate and fragility parameters of several metallic glass alloys.

5. CONCLUSION

The metallic glass-forming alloy, $Pd_{43}Ni_{10}Cu_{27}P_{20}$, was studied for this thesis. The thermophysic properties of this sample were characterized including crystallization behavior by means of the TTT-diagrams. The specific heat capacity was measured by DSC. Thermodynamic functions, enthalpy, entropy, and Gibbs free energy, can be calculated using the difference of specific heat capacity between liquid and crystalline state. As a result of the calculation of the above thermodynamic functions, the high glass forming ability for this sample was proved. The small driving force, Gibbs free energy difference between liquid and solid state, small entropy of fusion, and big T_{rg} value are evidence for a high ability of glass formation. Viscosity, not measured in this study, is another parameter that affects glass-forming ability. However, from Figure 25, and 26, it can be expected indirectly that the values of viscosity also indicate a high glass-forming ability of system. The high fragility parameter, which is shown in Figure 25 and 26, means that the alloy is a strong-liquid. This means the viscosity and the kinetics of this sample stays sluggish in the supercooled liquid regime compared to other metallic glass-forming alloys in the liquid state.

What happened to the $Pd_{43}Ni_{10}Cu_{27}P_{20}$ alloy with heat treatment around glass transition was clarified by observing glass transition shift. It can be seen in Figure 24, that the sample undergoes the glass transition at two different temperatures before it crystallizes. The decomposition in this sample was determined by the existence of

two glass transition temperatures. Microscopically, phase separation has not been observed and discussed. It is suggested that further study of decomposition of the $Pd_{43}Ni_{10}Cu_{27}P_{20}$ alloy by the X-ray powder diffraction (XRD) and the transmission electron microscopy (TEM) is necessary to clarify the decomposition in the system and the influence on nucleation and growth.

BIBLIOGRAPHY

[1] Klement, W., Willens, R. H., and Duwez, P. 1960. "The formation of non-crystalline Au-Si alloys by rapid quenching," *Nature* 187: 869-872 .

[2] Zhang, T., Inoue, A., and Masumoto, T. 1993. "The effect of transition metal (TM)on the supercooled liquid region for (Zr0.7Cu0.3)90TM10 amorphous alloy," *Journal of Material Science Letter* 12:700-701.

[3] Peker, A., and Johnson, W. L. 1993. "A highly processable metallic glass: $Zr_{41.2}$-$Ti_{13.8}Cu12.5Ni_{10.0}Be_{22.5}$," *Applied Physic Letters* 63:2342-2344.

[4] Kim, Y. J., Busch, R., Johson, W. L., Rullison, A. J., and Rhim, W. K. 1994. "Metallic-glass formation in highly undercooled $Zr_{41.2}Ti_{13.8}Cu_{12.5}Ni_{10}Be_{22.5}$ during containerless electrostatic levitation processing," *Applied Physics Letters* 65:2136-2138.

[5] Turnbull, D., and Cohen, M, H. 1961. "Homogeneous nucleation of crystals from simple liquids," *Nature* 189:131-133.

[6] Inoue, A. 1995. "High-strength bulk amorphous-alloys with low critical cooling rates," *Material Transaction JIM* 36:866-875.

[7] Greer, A. L. 1995. "Metallic Glasses," *Science* 267:1947-1953.

[8] Lu, L. –R., Wilde, G., Gorler, G. P., and Willnecker, R. 1999. "Thermodynamic properties of Pd-based glass-forming alloys," *Journal of Non-Crystalline Solids* 251:577-581.

[9] Schroers. J., and Johnson. W. L. 2000. "Crystallization of $Zr_{41}Ti_{14}Cu_{12}Ni_{10}Be_{23}$," *Materials Transaction JIM* 41:1530-1537.

[10] Schroers. J., Busch. R., and Johnson. W. L. 2000. "Crystallization kinetics of the Bulk-glass-forming $Pd_{43}Ni_{10}Cu_{27}P_{20}$ melt," *Applied Physics Letters* 77:1158-1160.

[11] Busch. R., Kim. Y. J., and Johnson. W. L. 1995. 7th International Symposium. "On Experimental Method for Microgracity Material," TMS meeting, Vegas, Feb.13-15.

[12] Kui. H. W., and Turnbull. D. 1987. "The heat capacity $Ni_{40}Pd_{40}P_{20}$ in the liquid, glass and crystallized states," *Journal of Non-Crystalline Solids* 94:62-69.

[13] Busch. R., Liu. W., and Johnson. W. L. 1998. "Thermodynamics and kinetics of the $Mg_{65}Cu_{25}Y_{10}$ bulk metallic glass forming liquid," *Journal of Applied Physics* 83:4134-4141.

[14] Kui. H. W., Greer. A. L., and Turnbull. D. 1984. "Formation of bulk metallic glass by fluxing," *Applied Physics Letters* 45:615-616.

[15] Kubaschewski. O., Alcock. C. B., and Spencer, P. J. 1993. Materials. New York: Permagon., pp. 78-82.

[16] Kouzmann. W. 1948. "Thermodynamics of liquids at large undercoolings," *Chemistry Research* 43:219-221.

[17] Angell. C. A. 1995. "Formation of Glass from Liquid and Biopolymers," *Science* 267:1924-1935.

[18] Nishiyama. N., Inoue. A. 1999. "Superccoling investigation and critical cooling rate for glass formation in Pd-Cu-Ni-P alloy," *Acta Materialia* 147:1487-1495.

[19] Angell. C. A., Richards. B. E., and Velikov. V. 1999. "Simple glass-forming liquids: their definition, fragilities, and landscape exitation profile," *Journal of Physics*: *Condensed Matter* 11:A75-A94.

[20] Waniuk. T. A., Busch. R., Masuhr. A., and Johnson. W. L. 1998. "Equilibrium viscosity of the $Zr_{41.2}Ti_{13.8}Cu_{12.5}Ni_{10}Be_{22.5}$ bulk metallic glass-forming liquid and viscous flow during relaxation, phase separation, and primary crystallization," *Acta Materialia* 46:5229-5236.

[21] Turnbull. D. 1969. "On the nucleation of crystals from liquids," *Contempt Physics* 10:473-476

[22] Busch R., Bakke. E., and Johnson. W. L. 1998. "Viscosity of the supercooled liquid and relaxation at the glass transition of the $Zr_{46.75}Ti_{8.25}Cu_{7.5}Ni_{10}Be_{27.5}$ bulk metallic glass forming alloy," *Acta Materialia* 46:4725-4732.

[23] Glade. S. C., Busch. R., Lee. D. S., Johnson. W. L., Wunderlich. R. K., and Fecht. H. J. 2000. "Thermodynamics of $Cu_{47}Ti_{34}Zr_{11}Ni_8$, $Zr_{52.5}Cu_{17.9}Ni_{14.6}Al_{10}Ti_5$ and $Zr_{57}Cu_{15.4}Ni_{12.6}Al_{10}Nb_5$ bulk metallic glass forming alloys," *Journal of Applied Physics* 87:7242-7248.

[24] Glade. S. C. 2000. "The $Cu_{47}Ti_{34}Zr_{11}Ni_8$ glass-forming alloy:Thermophysical properties, crystallization and effect of small alloying additions on the thermal stability," Material Science Doctor of Philosophy, California Institute of Technology. pp. 28.

[25] Scheider. S., Thiyagarajan. P., and Johnson. W. L. 1996. "Formation of nanocrystals based on decomposition in the amorphous $Zr_{41.2}Ti_{13.8}Cu_{12.5}Ni_{10}Be_{22.5}$," *Applied Physics Letters* 68:493-495.

[26] Macht. M. P., Wanderka. N., Wiedenmann., A., Wolleaberger. H., Wei. Q., Fecht., H.J., and Close. S. G. 1996. "Decomposition of the supercooled liquid of the bulk amorphous alloy $Zr_{41}Ti_{14}Cu_{12.5}Ni_{10}Be_{22.5}$," *Material Science Forum* 225:65-70.

[27] Liu. W. S, Johnson. And W. L. 1996. "Precipitation of bcc noncrystals in bulk Mg-Cu-Y amorphous alloys," *Journal of Materials Research* 11:2388-2392.

[28] Lu, L. R., Wilde, G., Gorler, G. P., Fecht. H. –J., and Willnecker, R. 2000. "Investigation of specific heat and thermal expansion in the glass-transition regime of Pd-based metallic glasses," *Journal of Non-crystalline Solids* 274:294-300.

[29] Loffler. J. F., Bossuyt. S., Glade. S. C., Johnson. W. L., Wanger . W., and Thiyagurajon. P. 2000. "Crystallization of bulk amorphous Zr-Ti(Nb)-Cu-Ni-Al," *Applied Physics Letters* 77:525-527.